Ocean Engineering 286 (2023) 115589

Contents lists available at ScienceDirect

Ocean Engineering

journal homepage: www.elsevier.com/locate/oceaneng

An Efficient Method for Design and Powering Prediction of Fast Slender Catamarans

John Martin Kleven Godø *, Sverre Steen, Odd Magnus Faltinsen

Norwegian University of Science and Technology, Department of Marine Technology, Otto Nielsens Veg 10, 7052 Trondheim, Norway

ARTICLE INFO

Dataset link: https://www.ntnu.edu/imt/software/fastships

Keywords:
Fast ferry
Catamaran
Hull series
Resistance model

ABSTRACT

This paper presents a parameterized and mathematically defined hull shape that can be tuned to represent modern passenger fast ferries. Additionally, a resistance calculation model for high-speed slender round-bilge catamarans is presented.

The resistance model builds on established theory, but incorporates novel contributions in the modeling of the wake hollow downstream of transom sterns and the form factors of slender catamarans. To generate systematic data on wake hollow length and form factors, 3D RANS simulations are employed, and the suggested models are evaluated by comparing them with these simulations.

A validation study is conducted, indicating that the resistance model can provide accurate results for typical fast ferry catamaran hulls at design draft and reduced drafts. Furthermore, it is shown that the combination of the proposed hull geometry and resistance calculation models can yield reliable predictions for the power requirement of existing vessels. This enables accurate power prediction in cases when limited hull geometry information is available. The hull geometry model is made available through open-source code.

1. Introduction

The high energy requirements of fast ferries per passenger-distance, coupled with the sensitivity of resistance to weight, pose significant challenges for transitioning to zero-emission power systems with larger mass per unit energy. The Norwegian fast ferry industry is under pressure to transition to low or zero emission operation. The first commercial route for a battery powered fast ferry recently started operation (TrAM, 2022), and several feasibility studies on zero-emission operation of longer routes have been conducted (Miljodirektoratet, 2019). Conclusions on the technical and economic feasibilities, and on whether conventional catamaran hull forms will be suitable for the task, are varied. To evaluate which routes might be suitable for zero-emission operation requirements, and the costs and benefits of such, decision makers require increased knowledge of current energy requirements and the feasibility of zero-emission solutions.

A fleet-wide feasibility study on the replacement potential for Norwegian fast ferries with zero-emission vessels was conducted by Sundvor et al. (2021). They evaluated both battery and hydrogen fuel cell power systems. This study made a simplified assumption that the vessels, except from the power system, were to remain identical to current vessels on the same routes. Since energy-specific and power-specific masses of zero-emission power systems is typically larger than that of conventional systems, zero-emission vessels will likely have larger displacement relative to passenger count. Furthermore, the increased cost and mass of zero-emission power systems will likely incentivize a stronger focus on optimizing hull designs and main dimensions for minimum energy consumption. Partly or fully foil supported designs might therefore become attractive. It is hence reasonable to explore the solution space of zero-emission fast ferries without the constraint of assuming the hull shape to be the same as for existing vessels.

To facilitate such analyses, and analyses of existing vessels, it is desirable to have a quick design and analysis tool for slender catamaran hulls which are representative of those of fast ferries. Since proprietary hull forms are used by industry, there is very limited information openly available on the details of such hull shapes. Consequently, it is desirable to develop a resistance model which requires only a minimum of input data on the hull in question. Furthermore, a numerically efficient model is needed, to facilitate its use in optimization of shape, main dimensions, trim, and other potentially relevant parameters for the energy efficiency of fast ferries. Additionally, numerical efficiency is key for allowing the use of the model in analyses and optimization of the take-off phase of hydrofoil vessels.

Current work presents a quick method for calculating the power requirement of vessels based on known speed profiles and limited information on hull shape. It is built upon the following sets of requirements. The model is to be based on first principles, allowing design exploration

* Corresponding author.
E-mail address: john.martin.godo@ntnu.no (J.M.K. Godø).

https://doi.org/10.1016/j.oceaneng.2023.115589
Received 25 April 2023; Received in revised form 7 August 2023; Accepted 8 August 2023
Available online 16 August 2023

List of Symbols

$\hat{S}$	Wetted surface of a demihull minus A_{TR}
∇	Demihull volume displacement
ρ	Water density
ρ_A	Air density
A_F	Frontal area of above-water parts of the vessel
A_L	Lateral area of above-water parts of the vessel
A_{TR}	Cross-sectional area of the submerged transom
B	Demihull width
$b_t(z)$	Width of transom at vertical coordinate z
C_B	Block coefficient
C_F	Frictional resistance coefficient
C_P	Pressure resistance coefficient
C_T	Total resistance coefficient
$C_{D,b,v}$	Drag coefficient of a ventilated transom
$C_{D,b,w}$	Drag coefficient originating from transom-stern pressure loss at a wetted transom
$C_{D,A}$	Air resistance coefficient
C_{F0}	Flat plate frictional resistance coefficient
C_{F0}	Flat plate frictional resistance coefficient
C_{Fm}	Model-scale frictional resistance coefficient
C_{Tm}	Model-scale total resistance coefficient
$C_{Y,A}$	Aerodynamic sideforce coefficient
D_A	Air resistance
$F_{Y,A}$	Aerodynamic sideforce
Fn	Froude number based on the waterplane hull length
$Fn_{Transom}$	Froude number based on submerged transom area
g	Acceleration of gravity
$H_{1/3}$	Significant wave height
k_F	Form factor, frictional resistance only
L	Demihull length
L_H	Wake hollow length
LCB	Longitudinal centre of buoyancy
$P(\hat{x})$	Blending function in the hull geometry model.
R	Resistance [N]
R_F	Frictional resistance
S	Wetted surface of a demihull
T	Demihull draft
T_0	Wave pectrum spectral maximum period
T_D	Demihull design draft
T_t	Transom submergence
U_A	Relative speed between the vessel and the surrounding air
U_S	Ship speed
U_W	Wind speed
$z_{c,b}$	Vertical area centre of the submerged transom

and optimization without reliance on empirical data sets such as those by Nordström (1951), Werenskiold (1990), Rambech (1998) or Førrisdal (2018). This allows new sizes, shapes, ratios of main dimensions or design speeds to be evaluated. Reliable resistance estimates are to be obtained for conventional modern fast ferries, to enable the evaluation of current energy use and emissions. Engineering accuracy is to be obtained for the resistance of hulls at reduced draft, representing foil supported operation or the take-off phase of hydrofoil catamarans. It must be quick-running, to allow fleet-wide evaluation of operating profiles and early-phase design exploration. A final requirement is that input and output data is to be familiar to a vessel designer, preferably allowing both high-level input in the form of main dimensions and more detailed input for a more flexible hull design process. We limit our model to slender catamaran hulls, since this is the main design principle applied in contemporary fast ferry design. At the end of 2020, 66% of all fast ferries in operation were based on catamaran hulls (Shippax, 2021).

These requirements indicate a two-part solution of creating a parametric hull geometry and a resistance model for analyzing it. The former must have properties which allow it to be tuned to a representative shape of modern fast ferries, while in other cases allow parametric modification of dimensions and geometrical features which might be important for resistance. This includes unconventional displacement catamaran forms, as well as forms representative for foiling catamarans (Minsaas, 1993; Jorde, 1991; Svenneby and Minsaas, 1992). The resistance model must be quick-running, simple, and well-validated, with results of engineering accuracy.

1.1. Geometry definition

For the hull geometry, we have identified four different paths in existing literature, which could theoretically have been taken. One option would be to utilize published hull series for high-speed displacement hulls and fast ferry catamarans, such as the Series 64 (Yeh, 1965), NPL (Marwood and Bailey, 1969; Bailey, 1976), Series 65 (Holling and Hubble, 1974), Series 89 (Müller-Graf, 1993; Müller-Graf et al., 2002), Delft 372 model/DUT Catamaran (van't Veer, 1998b,a), or a collection of "typical hull forms" for Australian fast ferries (Sahoo et al., 2004). However, the use of such hull series and predetermined geometries does not meet our requirements for two main reasons. Firstly, most of these series have geometrical features that differ significantly from modern fast ferry hulls, making it unlikely that their resistance curves are representative for these. The Series 64 comprises inwards-sloping sections above the waterline and highly convex cross-sections in the bow, while the Series 65 has hard chines in parts of the hull. The Delft 372 does not have a submerged transom-stern. In addition, most of the hull series shapes include:

- V-bottomed sections through large parts of the hull, not constrained to the bow
- Relatively steeply sloped keel line in the aft ship.
- A significantly forward-sloping stem, as opposed to near-vertical or even backwards-sloping stems in many newbuilds.
- Narrowing width towards the stern
- Lower slenderness ratios, $L/\nabla^{1/3}$, where ∇ denotes volume displacement.

Secondly, these hull series lack complete parameterization, limiting their use in case studies or optimization efforts of hull shapes. Therefore, it is deemed more reasonable to start from scratch and create a fully mathematically defined and parameterized hull shape.

A different path taken in previous works is the definition and optimization of catamaran hulls by spline-based interpolation surfaces (Subramanian and Joy, 2004; Cyberiad, 2015; Vernengo and Brizzolara, 2015; Kanellopoulou et al., 2019; Papanikolaou et al., 2020; Mittendorf and Papanikolaou, 2021). This gives outstanding freedom to shape the hull and was shown in some works to form a good basis for design optimization. It does however come with some drawbacks in the setting of our use case. One is that there is a need for manual inspection of the "fairness" of the lines (Subramanian and Joy, 2004). Smoothing procedures could be implemented to overcome this challenge, but that would make the design process less intuitive through

Table 1
Summary of hull geometry models in previous works.

Type	References	Advantages	Disadvantages
Hull series	Yeh (1965) Bailey (1976) Marwood and Bailey (1969) Holling and Hubble (1974) Müller-Graf (1993) Müller-Graf et al. (2002) van't Veer (1998b) van't Veer (1998a) Sahoo et al. (2004)	Very little hull data required	– Shapes are not representative of modern fast ferry hulls. – Little flexibility for parametrical tuning of the geometry
Spline-based interpolation surfaces	Subramanian and Joy (2004) Vernengo and Brizzolara (2015) Kanellopoulou et al. (2019) Papanikolaou et al. (2020) Mittendorf and Papanikolaou (2021) Cyberiad (2015)	Large geometrical freedom	– Requires manual intervention and tuning – Typically not defined by main dimensions or other intuitive parameters
Section data specification	Cyberiad (2015)	Less manual intervention and fairing of lines, as compared to a control-point-and-spline- based geometry	– Limited geometrical freedom – Typically not defined by main dimensions or other intuitive parameters
Mathematical descriptions from a small number of key parameters	Day and Doctors (1997)	– Very little hull data required – Highly tunable geometry	– Existing versions do not represent the shapes of modern fast ferry hulls.

the automatic alteration of hull details based on breakage of curvature or other criteria. Furthermore, a spline-based hull shape, which is inherently an interpolation of a set of control points, prevents quick and simple definitions of a hull through specification of parameters which are intuitive for a naval architect or hull designer. Examples of the latter are length, width, draft, entrance angle, and the depth of the transom stern. Several of the mentioned studies also come with the limitation that they are software-specific, with the models existing only inside the CAESES® geometry optimization software by FRIENDSHIP SYSTEMS (Friendship Systems, 2023).

Additionally, one might argue that the great freedom that comes with a spline-based surface description is not strictly necessary. Couser et al. (1997) showed that, for relevant fast ferry Froude numbers of 0.7 and greater, less than 30% of the total resistance can be attributed to wavemaking. This was further supported in a recent study by Mittendorf and Papanikolaou (2021). A low share of wavemaking drag would advocate for a relatively simple model for the hull shape, where a medium level of details can be tuned. These details should include the longitudinal distributions of width, draft and section shape (within strict limitations), while not necessarily allowing "random" shapes defined by point clouds. This is because there is likely little to gain from altering local curvatures or local geometrical peculiarities in an attempt to reduce wavemaking drag, while there might be a lot to gain from simple modifications for reducing wetted surface area or submerged transom area. This is further supported by the findings of Papanikolaou et al. (2020), where the drag minimization result of an impressive optimization study of a zero-emission fast ferry hull was superseded by more than 10% when a single design constraint on the demihull beam was relaxed. No optimization was mentioned for the latter hull shape. This indicates that the overall design parameters, such as the ratios of the main dimensions, are far more important for the resulting resistance, than are detailed geometrical modifications.

The resistance calculation code Michlet (Cyberiad, 2015) has taken a third path to hull geometry description. It allows a hull to be designed through the specification of parameters for longitudinal position, width, draft, and shape of a set of hull sections. Up to nine sections can be described, requiring in that case 42 parameters to be set. This approach reduces the freedom and requirement for attention to detail connected with a control-point-and-spline-based hull geometry. It is however a challenging job to represent a modern fast ferry hull shape with the limited number of allowable sections. The specification of parameters is arguably also not as intuitive as it could be, as in practice it demands a series of manual adjustments and visual inspections in order to get a smooth hull that satisfies a set of requirements on its key properties, for example a desired maximum beam, draft, entrance angle, stern profile slope, and center of buoyancy.

A fourth path, constituting an important contribution to the simple hull geometry specification for slender catamarans, was taken by Day and Doctors (1997). They used a mathematically defined hull shape, inspired by the Wigley hull (Wigley, 1942), to describe forward/aft symmetric hulls. The geometry comprised a constant-section midship and the possibility of vertical sides from below the waterline, thereby better resembling realistic hull shapes than what is the case for the Wigley hull. Several aspects of the geometry do however distinguish it from that of modern fast ferry hulls. This includes forward/aft symmetry, V-bottomed sections throughout the whole length of the hull, a parametric width distribution and the lack of a transom stern. It also lacks parameters for the direct prescription of the keel line angle of the aft ship and the waterline entrance angle of the fore ship, and no above-water geometry is included.

The different approaches to high-speed catamaran hull geometry specification from previous works are summed up, including notes on advantages and disadvantages, in Table 1. None of these seem to fit our needs. We have therefore developed our own parameterized and mathematically defined hull model for high-speed displacement catamarans. This can both be tuned to represent the shape of modern fast ferries, and is suited for optimization, parameter and case studies of future zero-emission fast ferries of various shapes and sizes. It takes intuitive high-level design parameters as input and provides an easy path to reasonable fast ferry hull shapes. Using the model, we also create a hull shape which is representative of modern fast ferries, allowing quick estimates of their power requirement at different sizes and speeds. The model is fully transparent, allowing reproducible calculations and case studies of existing or future fleets without the use of proprietary hull geometries. Example geometries and software tools for generating the geometry have been made available online (Godø and Steen, 2023).

The geometry model herein can be viewed as an adaptation and further development of the approach of Day and Doctors (1997), specifically tailored to the use case of fast ferry hulls of the early 21st century. It allows a gradual transition from V-shaped to U-shaped sections from the bow to the stern, a transom stern of specified submergence, the specification of the keel line and waterline entrance angles, convex fore ship waterlines, a realistic keel line slope with constant fore ship draft and a smooth transition to a shallower draft at the stern, and the addition of a realistic above-water geometry.

1.2. Resistance model and its validation

Significant efforts have been made on the quantification of the relative importance of resistance parameters of slender catamarans, as well as validating numerically efficient resistance calculation models (Molland and Lee, 1997; Doctors and Day, 1997; Couser et al., 1997, 1998a,b; Zhang et al., 2015; Mittendorf and Papanikolaou, 2021). These works do however highlight a lack of consensus on two aspects of the calculations, namely modeling of the wake hollow downstream of transom sterns and the magnitude of form factors for slender catamarans. More details are given under respective headlines of Section 3.

The presented resistance model builds upon the mentioned works. New knowledge is added on the topics of wake hollow modeling and form factors, in the form of new RANS data, simplified models and evaluation of the accuracy of the latter. Extensions are also added to account for air resistance and added resistance due to wind.

A key part of current work is the validation of the resistance model for geometries and operating conditions which are relevant for modern fast ferries. We also include reduced-draft operation, representing foil-supported hulls or hydrofoil catamarans in the take-off phase. There seems to be a lack of published resistance data on hull shapes which are representative of modern fast ferries, specifically of hull shapes of sufficiently high slenderness ratio. We have therefore used the hull geometry model to create what we believe to be a representative shape, and performed resistance simulations using RANS software. The results are used for evaluating the accuracy of the resistance calculation code on a realistic hull. RANS-based benchmark data is also used for validation at reduced drafts.

A study is also included, in which we evaluate the correspondence between results generated with a combination of the presented hull geometry and resistance models, and experimental results on the resistance of a modern fast ferry. This constitutes a validation of the ability of the combined models to predict the resistance of existing vessels.

1.3. Structure

This paper is divided into three main parts. Section 2 presents the hull geometry model. The resistance calculation model, including novel contributions on the modeling of the wake hollow and on form factors for slender catamarans, is presented in Section 3. Following a brief verification study in Section 4, Section 5 presents validation studies of the resistance model, as well as of the RANS simulations. Here we also present the comparison with resistance data of a modern commercial fast ferry. The RANS simulations are performed using OpenFOAM, and they are used to study flow physics and to obtain relevant resistance-related values, as outlined in detail in Section 3, 4, and 5.

To limit the length of the paper, we have separated some content of secondary importance into appendices. Appendix A presents the reasoning behind the choice of hull geometry parameters used when creating what we believe to be a representative modern fast ferry hull. All details regarding the RANS simulation setup and the evaluation of the numerical accuracy of the RANS simulations are presented in Appendix B. The NPL hull geometry was used in parts of the validation study, and a set of assumptions had to be made in order to create this from published data. These are presented in Appendix C.

2. Hull geometry model

This section presents a hull geometry model which takes simple inputs which define the longitudinal distribution of the waterplane width, draft, and cross-sectional shape, and outputs a three-dimensional hull mesh. Every point on the hull surface is mathematically defined from these parameters. This is done by scaling the cross-sectional shape to the desired width and draft at each longitudinal position. Both submerged and above-water parts of the hull are included. The following sections describe the design model, and the input required to fully define a hull.

As we shall see in Section 5.2, the model can be used to create hull shapes with very similar resistance properties to those of modern fast ferries. It has been implemented in the software package FASTSHIPS (Fast And Simple Tool for Simulation of HIgh Performance Ships), which is under development by the Department of Marine Technology at the Norwegian University of Science and Technology (NTNU). The geometry model has been made available under an open-source licence to facilitate its future use (Godø and Steen, 2023). All results herein were generated with FASTSHIPS v1.0.0.

2.1. Input

The waterplane width and draft, and cross-sectional shape parameters, are specified at a limited set of longitudinal positions. The software then makes smooth interpolations between these. Unless otherwise specified, the transitions are made by the blending function defined by Eq. (1), with $F(\hat{x})$ as given by Eq. (2). $\hat{x} = (x - x_0)/(x_1 - x_0)$ defines the dimensionless distance along the blending region, x_0 and x_1 define the longitudinal start and end positions of the blending region and P denotes the parameter being blended. The blending function yields smooth transitions with continuous first derivatives.

$$P(\hat{x}) = P_{x_0}(1 - F(\hat{x})) + P_{x_1} F(\hat{x}) \tag{1}$$

$$F(\hat{x}) = 1 - 0.5(1 + \cos(\pi \hat{x})) \tag{2}$$

2.1.1. Waterplane width

The longitudinal distribution of the waterplane width is defined by three parameters: the bow entrance angle, the relative longitudinal position of the fore shoulder, and the maximum width. The waterplane width is assumed constant astern of the shoulder. Eq. (1) is used to create a smooth transition between a constant-entrance-angle bow region and the constant-width region. An example distribution of waterplane width is shown in Fig. 1(a), where B denotes the waterplane width.

2.1.2. Draft

Draft varies through three longitudinal regions: a bow region, a constant-draft midship region and a stern region. These are defined by the following parameters:

- T_{max}/L_{WL}
- $T_{transom}/L_{WL}$
- Relative length of the midship constant-draft region
- Relative length of the aft transition region
- Stern keel line slope
- Bow region superellipse power.

T_{max} and $T_{transom}$ define the maximum and transom drafts, respectively, while L_{WL} denotes the waterline length at the design draft. “Relative length” denotes length relative to L_{WL}. The keel line at the transom slopes by the specified angle. Eq. (1) is used to create a smooth transition between the constant-draft midship region and the constant-slope transom values, through a region of user-specified relative length. In the bow region, the keel line follows the shape of one quadrant of a superellipse. An example of a longitudinal draft distribution is given in Fig. 1(c).

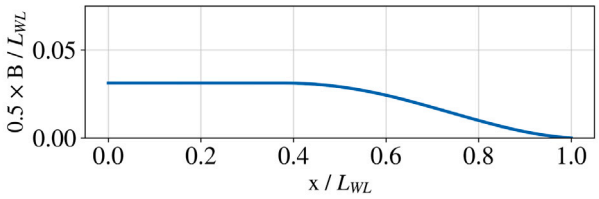

(a) Waterplane halfwidth relative to the hull length at the waterplane.

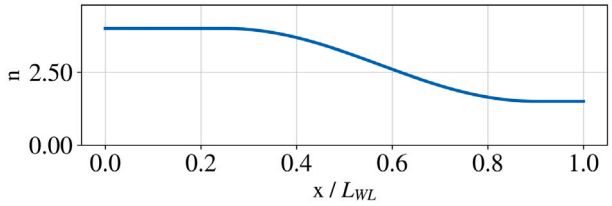

(b) The power of the superellipse defining the cross-sectional shape

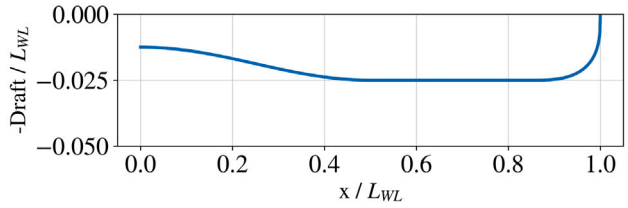

(c) -Draft relative to the hull length at the waterplane.

Fig. 1. Longitudinal distributions of waterplane width, draft, and the power of the superellipse defining the cross-sectional shape.

2.1.3. Cross-sectional shape

The cross-sections of the submerged part of the hull are defined by superellipses, as mathematically described by Eq. (3). In a cross-sectional coordinate frame where x goes in the transverse direction and y in the vertical direction, a denotes the demihull half-width and b denotes its draft. The submerged cross-section is found as the negative-y halfplane of the superellipse. By varying n, the *power* of the superellipse, we can vary the cross-sectional shapes from concave V-shapes, via straight and V-shapes, convex V-shapes and rounded-bilge shapes, to near-rectangular sections. Examples of cross-sectional shapes at various values of n are shown in Fig. 2.

$$\left|\frac{x}{a}\right|^n + \left|\frac{y}{b}\right|^n = 1 \tag{3}$$

The cross-sectional shapes are defined by a longitudinal distribution of the power of superellipse section shapes n. Constant values are set in the bow and stern regions, between which Eq. (1) creates a smooth transition. The following parameters are tunable:

- Relative length of the forward constant-n region
- Forward region value of n
- Relative length of the aft constant-n region
- Aft region value of n

An example of a longitudinal distribution of the cross-sectional shape parameter n, generated with the hull geometry model, is shown in Fig. 1(b).

The above-water shape of the hull sections is modeled after the shapes found in modern fast ferries. It features a flare that extends outwards from the design waterline as a quadratic function of the vertical position, up to a specified maximum flare width and flare height. Above this point, the hull is extruded vertically to a specified deck height.

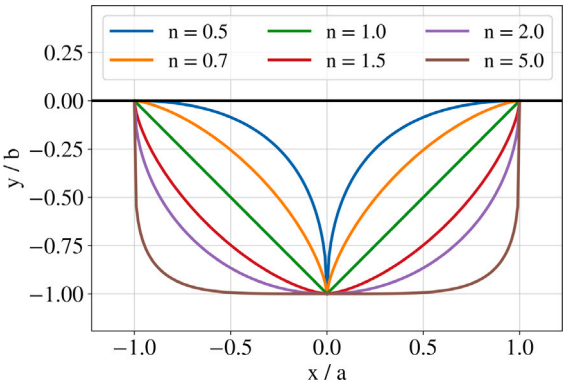

Fig. 2. Superellipses with varying values of the power n, as defined by Eq. (3).

The flare width and flare height are constant from the transom to a specified longitudinal position. Forward of this, the flare width reduces as a superelliptic function of the longitudinal position to zero at the bow, and the flare height increases as a quadratic function of the longitudinal position to a specified bow value. Examples of sections generated with the hull model can be seen in Fig. 3(a). The geometry above $z/L = 0$ is above water at the design draft. The above-water sections are described by the following parameters:

- Height to the main deck
- Maximum flare width
- Flare height in the aft region
- Relative length of the aft flare region
- Superellipse power n for the forward flare width transition.
- Flare height at the bow

2.1.4. High-level input

The software implementation of the geometry model, FASTSHIPS Hull Geometry, has the option of taking high-level input on the main dimensions of a hull. It thereafter generates a hull shape based on predetermined ratios of the above-mentioned dimensions. Two alternative input formats are permitted. One format takes the L_{WL}/B, B/T and T_t/T ratios together with L_{WL} as input, while the other takes these ratios together with the volume displacement. L_{WL} and B denote the waterplane length and width, respectively. This reduces the flexibility of the shapes that can be generated, but opens the possibility of using the software without any knowledge on hull design

2.2. Output

As the hull geometry model is mathematically defined, any geometry output format is theoretically possible. The software implementation currently supports the export of mesh files in the *Wavefront* format. This is a widely used mesh format, originally developed by Wavefront Technologies, which can be imported by several RANS software packages, visualization tools, 3D printing software, and by the resistance model presented in Section 3. Furthermore, section drawings, waterline drawings, and text files with the main geometric and hydrostatic parameters can be exported. A render of an exported mesh is shown in Fig. 4, while exported sections and waterlines can be seen in Fig. 3.

3. Resistance model

Extensive work has previously been devoted to the analysis of catamaran resistance. The resistance model presented herein builds on established theory, with new data and modeling contributions on the topics of wake hollow shape and form factors of slender catamarans.

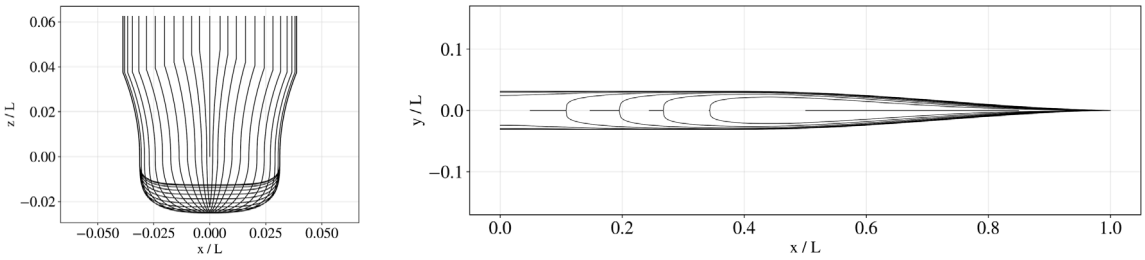

(a) Sections (b) Waterlines

Fig. 3. Hull model sections and waterlines example. The lines are for the NTNU FF1 hull, for which details are given in Appendix A..

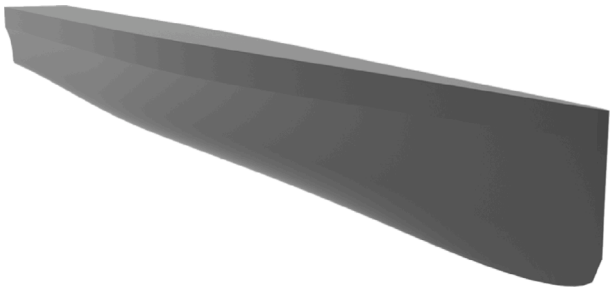

Fig. 4. Perspective view of output mesh from the hull model.

Our main focus is to achieve as simple a model as possible, while still retaining sufficient accuracy for engineering purposes. Focus is put on resistance estimates of modern and future conventional passenger fast ferries, which are assumed to have slender catamaran hulls that operate at $0.6 < Fn < 1.0$ at infinite depth. Fn is defined in Eq. (4), where U, g and L_{WL} denote forward speed, the acceleration of gravity, and ship length at the waterplane, respectively.

$$Fn = \frac{U}{\sqrt{gL_{WL}}} \tag{4}$$

The current section presents a simple theoretical method for performing resistance estimates of these vessels, followed by a validation study which evaluates its accuracy. This is done at the design draft and at reduced drafts. The resistance model sums the contributions from a set of components which are assumed to be independent. Models for each are presented in the following sections.

3.1. Wavemaking resistance

A review of published literature has revealed an interesting property of the relative magnitudes of resistance components of fast ferry catamaran hulls, justifying a major simplification. Couser et al. (1997) showed that most of the resistance of a slender catamaran at $0.6 \leq Fn \leq 1.0$ was constituted by frictional resistance. This trend was confirmed by the results of Jamaluddin et al. (2013), Shi et al. (2021) and Mittendorf and Papanikolaou (2021). In the latter, less than 10% of the resistance of a modern slender-catamaran fast ferry was shown to be wavemaking resistance at a typical service Froude number of 0.9. The very high slenderness ratios of modern fast ferries, as discussed in Appendix A, indicate an even stronger trend towards friction-dominated resistance than that found by Couser et al. (1997). Larger coefficients of wavemaking resistance have been observed at lower Froude numbers around 0.5 (Molland et al., 1994a; Couser et al., 1997; Jamaluddin et al., 2013; Shi et al., 2021; Mittendorf and Papanikolaou, 2021). Since most fast ferries spend most of their time at higher Froude numbers, and the power requirement is roughly proportional to U^3, the accuracy of the wave-resistance calculation at these speeds is less important for the total energy requirement on a route. This motivates the use of a relatively simple and numerically efficient model for wavemaking resistance.

Tuck (1987) presented a practical formulation of Michell's thin ship theory (Michell, 1898), in which hull geometry offsets were used directly instead of requiring the longitudinal derivative of such. He compared predictions of wavemaking resistance from the theory with various experiments, with which agreement was good. The resistance model uses these formulations directly in the prediction of wavemaking resistance. Input is given in the form of hull mesh files in the Wavefront format, and a pre-processing step splits the hull into a set of strips of equal vertical resolution.

3.1.1. Wake hollow model

In the wave resistance calculation method of Tuck (1987), there was no explicit mention of how to deal with submerged transom sterns. A generally accepted approach is to add a pointed-stern virtual appendage downstream of the transom (Faltinsen, 2005), calculating the wavemaking resistance on the hull including the extension. By assuming the shape to be equal to the shape of the water surface downstream of a ventilated transom stern, one implicitly assumes atmospheric pressure on the extension.

To the knowledge of the authors, there are no established and generally accepted standard procedures for calculating the shape and length of the wake hollow. Molland, Wellicome and Couser (Molland et al., 1994b; Couser, 1996; Couser et al., 1998b) presented a method in which the length was a given number of hull halfwidths at the stern. They referred to previous work on backwards-facing steps, implicitly assuming the flow not to ventilate downstream of the transom. This gave satisfactory agreement with experimental data in many cases, although tuning the number of halfwidths as a function of Fn was shown to improve correspondence with experiments (Couser, 1996; Couser et al., 1998b). The optimum tuning factors varied in magnitude by a factor of more than two, indicating that the model did not capture all relevant physics.

Doctors and Day (1997) proposed a method in which lines were drawn between points at the transom and a virtual focus point of the "rooster tail", calculated as a weighted average of crossing points of two-dimensional lines from the transom following a parabolic trajectory. They proposed that the trajectory from each point follows a gravitational-acceleration-driven trajectory, in which the latter is modified by a factor. The factor was 1 in the original publication. The magnitude of the overall wave resistance was finally scaled by a separate factor. This gave good correspondence with experimental data. Taravella et al. (2012) proposed a different gravity-acceleration-driven model, in which the trajectory was inverted and followed the path of a particle "falling" from the aftmost end of the wake hollow to the bottom of the transom, with a speed equal to the negative of the vessel speed.

Armstrong (2000) performed measurements of the length of the transom-stern hollow on a full-scale catamaran fast ferry in operation. Data were collected for a range of Froude numbers between 0.5 and 1.0. No variations of other operating conditions or the geometry were done,

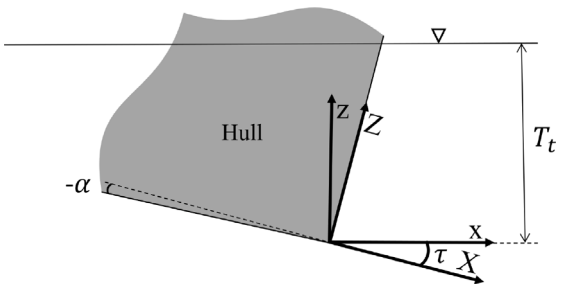

Fig. 5. Coordinate systems and parameters that are used in the wake hollow model.

Table 2
Main particulars of the hull shapes used in direct validation of the resistance model for slender hulls.

	NPL 4a, S/L = 0.2	*NTNU FF1*
L/B	10.4	16.0
B/T	1.5	2.5
$L/\nabla^{\frac{1}{3}}$	7.40	10.69
C_B	0.397	0.524
$LCB[\%]$	43.6	40.7
S/L	0.2	0.2

however, the vessel was free in trim and sinkage during the measurements. Armstrong pointed out that there is significant uncertainty in the measured values, since the ship wave pattern, waterjet outlet flow and large amounts of spray complicated the identification of the end of the wake hollow. Based on his data, he proposed that the length of the wake hollow can be estimated by Eq. (5), where $Fn_{Transom}$ is defined by Eq. (6), and L_H and A_{TR} denote the length of the wake hollow and the submerged area of the transom, respectively. The formula implicitly assumes the length of the wake hollow to be proportional to both $A_{TR}^{1/4}$ and $A_{TR}^{1/2}$, but since no variation of $A_T R$ was tested, it is hard to say whether this assumption holds. Armstrong listed this topic as one which would benefit from further work.

$$L_H = \sqrt{A_{TR}}(0.5 Fn_{Transom} + 2.6) \tag{5}$$

$$Fn_{Transom} = \frac{U}{\sqrt{g\sqrt{A_{TR}}}} \tag{6}$$

(Faltinsen, 2005) showed from Bernoulli's equation that the centreplane flow downstream of the transom can be described as in Eq. (7). X and Z denote tangential and normal directions to the keel line, U_S denotes ship speed and A is an unknown constant. The relevant coordinate system is shown in Fig. 5. By fitting the model to an empirical formula based on planing hull experiments (Savitsky, 1988), he could create expressions for the centerline surface shape as functions of trim angle, width, and speed. These expressions are however only applicable to planing hull forms and are limited to relatively steep trim angles of $6° < \tau < 14°$, where τ denotes the trim angle.

$$Z = \frac{A}{U_S} X^{3/2} \tag{7}$$

Other works include the experimental and numerical investigations by Lugni et al. (2004b,a), Maki et al. (2007, 2008), although at lower $Fn_T = U/\sqrt{gT_t}$ than those typical for fast ferries at design speed. T_t denotes transom draft, as illustrated in Fig. 5. Doctors (2015) proposed a regression formula for the length of the transom hollow based on experimental results at $Fn_T \leq 4$. A typical modern fast ferry might have a design speed of 30–35 knots and a transom submergence of approximately 0.5 m, yielding $7.0 \leq Fn_T \leq 8.1$. We are hence reluctant to using results from these studies in our model.

We will investigate an approach inspired by Faltinsen (2005), Doctors and Day (1997), and Taravella et al. (2012). Our approach is based on a hypothesis that, if the transom width is large relative to its submergence, the water surface close to the centreplane follows a predictable two-dimensional trajectory. Its shape is assumed to be in accordance with the derivation of Faltinsen. As opposed to the methods of Doctors and Day (1997) and Taravella et al. (2012), we hypothesize that the vertical acceleration of water in the wake hollow is dependent on the transom submergence. The latter determines the hydrostatic pressure in the proximity of the bottom of the transom, and hence affects the vertical pressure gradient forcing the water upwards downstream of the transom. Although he did not perform systematic studies of the effects of varying the transom submergence, some support for this can be found in the observations of Savitsky (1988). He found that the centerline profile obtained steeper slopes when operating at higher length-width ratios, all other parameters being equal. Since the width, the deadrise angle, and the trim angle were equal, our interpretation of his data is that he must have increased the draft to obtain the higher length-width ratios. Hence, his observation indicates a trend that the water surface trajectory in the wake hollow centerline obtains steeper slopes at deeper transom submergences. Wang et al. (2022) found that the length of the transom-stern hollow of a planing catamaran was practically unaffected by the displacement of the studied vessel. This further supports the theory that the steepness of the centreplane water surface trajectory in the wake hollow increases with increased transom draft. In this case, the increased slope must have been of a magnitude that corresponded to maintaining a constant wake hollow length when the draft changed.

Putting this in the context of the derivation of Faltinsen (2005), it means that the unknown coefficient A in Eq. (7) must be a function of T_t. We assume, inspired by the observations of Wang et al. (2022), that the length of the transom hollow is independent of the transom submergence if $\tau' = 0$, where $\tau' = \tau + \alpha_s$. τ denotes the vessel's trim angle and α_s denotes the local angle between the keel line at the stern and the horizontal plane. This implies $A(T_t) = \hat{A}T_t$. T_t denotes transom draft and $\hat{A}$ is an unknown constant. Transforming Eq. (7) into a coordinate frame of the same origin, but rotated so that x and y follow the global horizontal and vertical directions, we obtain Eq. (8). The parameters τ and α and the new coordinate system are illustrated in Fig. 5. We have assumed small values of τ' so that $\sin\tau' \approx \tau'$ and $\cos\tau' \approx 1$. The length of the wake hollow can be found by inserting $z = T_t$ and solving for x.

$$z = \frac{\hat{A}T_t}{U_S} x^{3/2} - \tau' x \tag{8}$$

To find the coefficient A, as well as to investigate the accuracy of the formula, we have conducted a series of Reynolds-Averaged Navier–Stokes (RANS) simulations in which we have varied the forward speed and draft. In this study, it was desirable to use a hull shape that is representative of that of modern fast ferries. For this purpose, we have tuned the input parameters of the presented hull model so that the output resembles that of modern relevant vessels. More details are given in Appendix A. The resulting hull shape is hereafter termed the NTNU Fast Ferry 1 (NTNU FF1), and its main particulars are given in Table 2. This hull shape was also used in Section 5.2, in which we compared resistance predictions from the combined hull geometry and resistance models, with that of experimental data on a modern fast ferry hull. Simulations were performed in 1:25 scale, with simulation settings as outlined in Section 5 and detailed in Appendix B.

For each RANS simulation, we measured the distance from the transom to the crossing point of the water surface at one of the demihull centerplanes with a horizontal plane at $z = 0.5T_t$. We choose this rather than measuring to z = 0, as we observed some cases where the "rooster tail" wave was lower than z = 0. The NTNU FF1 hull has $\tau' = 0$. Solving Eq. (8) for $\hat{A}$ at $z = 0.5T_t$, we obtain Eq. (9) for $\hat{A}$. $x_{z=0.5T_t}$ denotes the horizontal distance from the transom to the point at which the water surface has risen halfway back to the undisturbed water surface.

$$\hat{A} = \frac{0.5U}{x_{z=0.5T_t}^{3/2}} \tag{9}$$

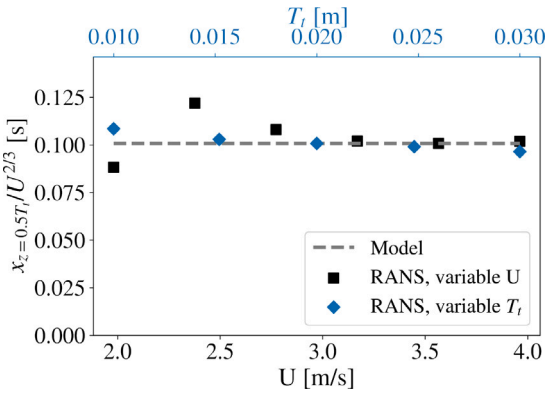

Fig. 6. Distance from the transom to the point where the water surface has risen halfway back to the undisturbed water level, divided $U^{2/3}$. Speed and draft variations.

$$x_{z=0.5T_t} = \left(\frac{0.5U}{\hat{A}}\right)^{2/3} = \tilde{A}U^{2/3} \tag{10}$$

With a representative value of $\hat{A}$, we can re-arrange Eq. (9) to predict the distance to $x_{z=0.5T_t}$, as presented in Eq. (10). $\tilde{A} = (0.5/\hat{A})^{2/3}$ is now a constant parameter. Fig. 6 shows the horizontal distance from the transom to the point at which the water level has risen halfway back to the undisturbed water level, divided by $U^{2/3}$, i.e. $\tilde{A}$. It includes RANS simulations and model simulations at varying speeds and submergences. Forward speed is varied so that $0.5 \leq Fn \leq 1.0$ and submergence is varied in the range $0.5T_{td} < T_t < 1.5T_{td}$. T_{td} denotes the design draft of the transom. $T_t = T_{td}$ in simulations with varying Fn and $Fn = 0.9$ when varying T_t. The value of $\hat{A}$ used in the model was chosen as the value for $Fn = 0.9$, $T = T_{design}$, where T_{design} denotes the design draft. $Fn = 0.9$ corresponds to $U = 3.57$ m/s. The full set of measured wake hollow length values can be found in Appendix D.

It is seen that the correspondence between the model and RANS results is very good for all speeds except $U = 2.38$ m/s. Investigating the shape of the flow field reveals that this case, together with the case of $U = 2.77$ m/s, has an unusually significant asymmetry of the wave elevation on the tunnel side versus the outside of the demihulls, close to the transom. It is noted that the length of a deep-water wave with phase velocity equal to U in these cases is 2.3 and 3.1 times the hull length. It is likely that the wave trough from the bow wave is close to the transom in these cases, and that interference effects between the hulls affect the magnitude of the resulting negative wave elevation on the inside of the demihulls. Significant asymmetry is observed in the shape of the transom hollows in these cases. This likely affects several aspects of the transom hollow shape, including its measured length. We are not attempting to capture such a level of detail in our model, and hence accept some error in the predicted length of the transom hollow at this data point.

The correspondence between the model and RANS results for variations in transom depth is very good for all data points. This supports our hypothesis of $A(T_t) = \hat{A}T_t$, meaning the wake hollow length remains constant through at least a relatively wide range of transom drafts. Several studies have found that $Fn_T = U/\sqrt{gT}$ is a determining parameter for the wake hollow length at lower Fn_T (Lugni et al., 2004b; Maki et al., 2007; Doctors, 2015). Our results indicate that, at the studied values of Fn_T, this parameter no longer determines the wake hollow length. Doctors (2015) presented a model on the form $x_{z=0} \propto U^{3.025}T^{-0.5125}$, where $x_{z=0}$ denotes the length of the wake hollow until crossing the undisturbed water surface. This was again based on observations at lower Fn_T. The model does not fit our data. These discrepancies with previous observations at lower Fn_T indicate that we are studying a regime of Fn_T in which significantly different flow physics are at play.

To obtain the three-dimensional (3D) shape of the wake hollow, we assume it to collapse inwards from the sides of the hull through a parabolic trajectory starting at the transom and ending at the crossing point between the centreplane water surface and the undisturbed water level. An alternative approximation of the 3D shape is also implemented, in the form of assuming a constant wake hollow width. The difference in the wavemaking drag predictions between simulations with these two shape models is shown in Section 5 to be very small. Both models provide only a rough approximation of the wake hollow shape observed from the 3D RANS simulations, and neither capture the local raise of the water surface in the form of a "rooster tail" downstream of the collapse of the wake hollow. However, as presented in Section 5, these inaccuracies do not yield significant errors in the resistance predictions.

3.1.2. Transom-stern pressure loss

Thin-ship theory calculates the wavemaking resistance as the radiated wavemaking energy, and hence does not integrate pressures over the wetted surface of the hull. In cases with a ventilated submerged transom stern, this means we do not account for the integral effect of having hydrostatic pressure on all submerged surfaces except the transom. We have therefore implemented two models for the transom-stern pressure loss. For ventilated sterns, we use the well-established approach of subtracting the loss of hydrostatic pressure by adding a resistance component $C_{D,b,v}$ as defined in Eq. (11). In this equation, $b_t(z)$ and $z_{c,b}$ denote the transom width at depth z and the vertical area center of the submerged transom, respectively. $C_{D,b,v}$ denotes the drag coefficient of a ventilated transom. This approach does not correct for the absence of dynamic pressure recovery.

$$C_{D,b,v} = \int_{z=T_t}^{0} \rho g z b_t(z) dz = \rho g z_{c,b} A_{TR} \tag{11}$$

For wetted sterns, we use an empirical formula by Hoerner (1965), originally formulated for the base drag of projectiles. It predicts the resistance on a base, as a function of the frictional resistance coefficient of the upstream body, by an empirical formula. The physical reasoning behind this approach is that one might view the negative dynamic pressure at a flat downstream surface normal to the flow as a result of the external flow pumping fluid out of the recirculation region downstream of the surface, by viscous shear forces along the edges of the recirculation region. The boundary layer acts as an "insulation region" between the internal and external flows. Its thickness, varying as a function of the upstream-body frictional resistance coefficient, determines the magnitude of the pumping. The formula was proposed for use in the estimation of base drag of ships by Steen and Minsaas (2014), in which it was re-written into a non-dimensional form equivalent to that of other resistance components typically dealt with in ship resistance. The resulting expression is given in Eq. (12). In this equation, $C_{D,b,w}$, S, and S_b denote the drag coefficient of the wetted transom and the wetted surface of the demihull, respectively.

$$C_{D,b,w} = 0.029\sqrt{(A_{TR}/S)^3/C_{F0}} \tag{12}$$

The choice of whether to use wetted or ventilated stern resistance coefficients is made automatically in the resistance model, by choosing the one that yields the lowest value. This is easily justified physically. If a wetted stern would be to yield higher resistance than a ventilated one, the average pressure on the transom would have to be lower than the atmospheric pressure. This would lead to ventilation of the transom stern. Oppositely, if the wetted-stern resistance formula predicts lower resistance than the one for ventilated sterns, this solution involves a higher average pressure than atmospheric. The flow would hence, in the absence of local pressure variations, not separate. Hysteresis effects on separation and re-attachment are neglected in the model.

3.2. Frictional resistance

The frictional resistance coefficient is calculated from the conventional approach of using a friction line and a form factor (28th ITTC Resistance Committee, 2017a). The resistance model is implemented with support for several friction lines, including the ITTC'57 and the lines of Grigson (1999), Katsui (2005), and Eça and Hoekstra (2008). It defaults to the formulation by Eça and Hoekstra (2008), which was used when generating all results herein. This line does not contain a baked-in form factor, as is the case for the ITTC'57 line.

A roughness allowance can be set, although this defaults to zero. Armstrong (2000) showed that the effect of adding a typical value of roughness allowance can be substantial, leading to a 6% decrease in top speed in an example case. Assuming a cubic relation between speed and power, this means an increase of engine power of 20% would be needed to maintain the original top speed in this case. To the knowledge of the authors, no systematic studies have been performed on the realistic roughness values to use in analyses of modern high-speed ferries with slender catamaran hulls. Armstrong concluded, based on advice from Peter van Oossanen and lectures by Burkhard Müller-Graf (Müller-Graf, 1994), that a roughness allowance of 0 for newly built aluminium or Glass-fiber Reinforced Plastic (GRP) hulls was reasonable. Modern fast ferries are typically constructed from either, alternatively from Carbon-Fiber Reinforced Plastic (CRP/CFRP), and the surface finish of the latter can safely be assumed to be equal to that of GRP hulls. We hence conclude that our standard value of zero roughness allowance is in accordance with common practice, but stress the fact that this might be a potential source of error when comparing with full-scale data. This is particularly so if such is obtained from a hull which was not recently cleaned from fouling.

ITTC (26th ITTC Propulsion Committee, 2011) gave a formula for calculating the roughness allowance from the roughness height. Model-tank practice indicates that a roughness height of 75 μm should be used for fast ferries.

3.2.1. Form factors

There seems to be a wide acceptance that form factors are important for the accurate prediction of the frictional resistance on slender catamaran hulls. There is, however, strong disagreement regarding the magnitude of such, and which factors might influence it. Molland et al. (1994a), Couser (1996), Couser et al. (1997) used a modified form factor on the form $(1 + \beta k)$ for catamarans, in which β denotes a modification due to interference effects between demihulls. For slenderness ratios above 7 they experimentally identified form factors in the range of 1.2–1.3 for monohulls and 1.4–1.5 for catamarans. An interpolation function for the results from Couser et al. (1997) was presented by Utama and Molland (2001). No systematic effects on the form factor from variations of demihull separation ratio were observed. The Froude number also had little effect on the values, while the slenderness ratio was found to be an important parameter (Couser et al., 1997). β was consistently observed to be above 1 (Molland et al., 1994a). In strong contrast to this, studies by Armstrong (2000) have identified form factors in the range of 0.94–1.3 for the same hulls as studied by Molland and Couser.

Both Molland and Armstrong used flat plate frictional resistance coefficients C_{F0} from the ITTC'57 friction line when defining their form factors. Armstrong claimed that the origin of the difference is that Molland incorrectly identified transom drag as part of the viscous resistance. Our view is more nuanced, and we would like to add that Molland never explicitly did so. In his experiments, he measured the wavemaking resistance with wave probes and subtracted these values from the total resistance to get the viscous resistance. It is judged likely that this might not have captured all the transom-stern resistance, as some of the energy from this dissipated through wave breaking and vortex creation in the wake hollow. This was addressed by Couser et al. (1997), and a re-calculation of the form factor for one of the experiments was done by subtracting the submerged-transom hydrostatic pressure loss forces from the total resistance. This did however only correct for approximately half of the discrepancy between the form factors of their earlier experiments and those presented by Armstrong (2000). An interesting note is that emerged-transom towing tests yielded form factors of 1.3–1.4 in the experiments of Couser (1996). This speaks strongly against the theory that the discrepancy between the results of Armstrong and Molland and Couser can be fully explained by a part-inclusion of the transom-stern resistance in the results of the latter.

Several causes of the discrepancies between Armstrong and Molland and Couser's form factors might be theorized. In addition to the possibility of an effect of transom-stern pressure drag, it is worth mentioning that the results of Armstrong are not exempt from a potential for errors. Some of his work was done with reflex models in a wind tunnel, in which the free surface was naturally not modeled. A fairing was also mounted downstream of the transom to approximate the shape of the wake hollow, potentially introducing errors in the velocity distribution along the hull and hence the value of the form factors. It was also pointed out in his work that blockage and interference effects with support structures were likely to have affected the catamaran results from the wind tunnel. Armstrong did RANS simulations as well. These had their own potential for error, the most obvious of which was the fact that only half a demi-hull was included in the computational domain. One hence implicitly assumed symmetric flow and wave elevation about each demihull. A hull fairing was again used downstream of the transom, instead of solving for the separation and free surface flow here. Wave elevations from a towing-tank test were imposed in the RANS simulation domain, potentially introducing errors from wave measurement inaccuracies.

The reasons for the discrepancies between reported form factors for catamarans seem not to have been fully resolved. Sahoo (Sahoo et al., 2004, 2007) reported that form factors seemed to be the least researched aspect of determining catamaran resistance.

Due partly to the apparent disagreement on the values of the form factors for catamarans, partly because our main focus is more slender hulls than those studied by mentioned authors, and partly because we want to use a friction line with no built-in form factor such as the ITTC'57 line, we choose to perform a study of form factors as part of current work.

The RANS simulations presented in Section 3.1.1 are re-used in this study. These are all performed on the same hull shape, operating at $0.5 \leq Fn \leq 1.0$, $0.75T_d \leq T \leq 1.25T_d$. T_d denotes the design draft of the hull. Altering the draft effectively alters the slenderness and B/T ratios of the hull, which vary from 9.68 to 12.28 and from 2.0 to 3.3, respectively. The hull operates at design draft in the cases with varying Fn, yielding slenderness and B/T ratios as presented in Table 2. The cases of varying draft were generated at $Fn = 0.90$. A frictional resistance coefficient was defined as presented in Eq. (13). In this equation, R_F and $\hat{S}$ denote the frictional resistance of the three-dimensional submerged hull and the wetted surface at standstill, minus the area of the submerged transom, respectively. The transom was ventilated in all the studied cases. Form factors were calculated as presented in Eq. (15), where C_{F0} was predicted by the friction line of Eça and Hoekstra (2008). The full set of resistance coefficients used when calculating the form factors is presented in Appendix D.

$$C_F = \frac{R_F}{\frac{1}{2}\rho U^2 \hat{S}} \tag{13}$$

$$k_F = C_F / C_{F0} - 1 \tag{14}$$

It is worth mentioning that the current approach of calculating the form factor implicitly includes a correction for the wave elevation on the frictional forces. This is because the frictional resistance extracted from the RANS simulations, R_F, accounts for the resistance on the instantaneous wetted surface, while C_F is non-dimensionalized with respect to the undisturbed wetted surface S.

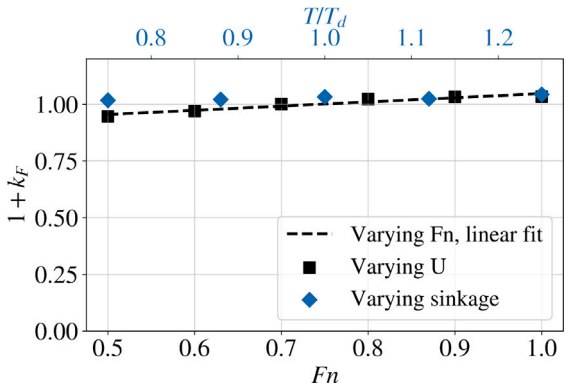

Fig. 7. The form factor of the NTNU FF1 hull as a function of *Fn* and relative sinkage. All results were obtained at 1:25 scale with the friction line of Eça and Hoekstra (2008).

The obtained form factors are shown in Fig. 7. All results are very close to $1 + k_F = 1$, with the lowest being $1 + k_F = 0.946$ for $Fn = 0.5$. An apparent trend of rising form factors with increasing *Fn* is observed. All values for varying drafts are above 1, with the highest being 1.043. The reason why form factors below 1 are possible is the fact that we have not accounted for wave elevation in the calculation of S. Another contributing factor to low form factors is that we have calculated these from the dimensionless frictional resistance, C_F, which does not include the viscous pressure resistance. The presented method involves no modeling of viscous pressure resistance. Its applicability is hence limited to vessels with transom sterns, for which there is limited pressure recovery at the stern and hence reason to believe that there is very little viscous separation and viscous pressure resistance.

A least-squares curve fit to a linear relation between *Fn* and k_F has been created, and is shown in Fig. 7. Although it fits the available data well, there is reason to believe it cannot be extrapolated to zero speed. The lower-*Fn* cut-off of the current dataset happens in a regime with a significant impact of ship-generated waves on the wetted surface, which will not be the case for *Fn* approaching zero. For lower *Fn*, we use a linear interpolation between $1 + k_F = 1.0$ at $Fn = 0$ and the value of the linear function at $Fn = 0.5$. This is done in the lack of better available data, bearing in mind that low-*Fn* accuracy is not the aim of the presented resistance model. For $Fn > 1.0$, we apply the value of the linear function at $Fn = 1.0$. It is evident from the data that the operational draft has very little effect on the form factor. We hence do not include this as a parameter in our form factor model. Our form factor equations, which are implemented in the resistance model and used in all results of Section 5, are given in Eq. (15).

$$\begin{aligned} k_F &= -0.0916Fn, && Fn < 0.5 \\ k_F &= -0.1378 + 0.184Fn, && 0.5 \leq Fn \leq 1.0 \\ k_F &= 0.0462, && Fn > 1.0 \end{aligned} \tag{15}$$

The almost constant value of the form factor through a wide range of drafts indicates that the data herein might be valid for many hull shapes, as long as the L/B-ratio is relatively close to that of the NTNU FF1 hull. The moderate effects of *Fn* on the form factor are in accordance with the findings of Couser et al. (1997). Furthermore, Couser found that the demihull separation had little effect on the form factor, indicating that our results can be used for various values of such.

3.3. Demihull interference

Two hulls in close proximity, however slender, will experience some interference. Molland et al. (1994a) reported that the form factor was consistently higher for catamarans than monohulls of equal hull shape. However, he found no systematic trend of this change with the separation ratio or forward speed. Similar results were reported by Couser (1996).

Both Molland et al. (1994a) and Couser (1996) reported steeper running trims for catamarans than monohulls, although (Couser, 1996) reported that the difference disappeared for $Fn >= 0.75$ and $Fn \leq 0.40$. Furthermore, different sinkages were reported for catamarans relative to monohulls, by both Molland et al. (1994a) and Couser (1996). These differences were not found to disappear past any *Fn* limit. The absolute value of the sinkage was however found to be relatively small for slender hulls, and was reported to be smaller at higher *Fn*. The effects of any hull interference on sinkage might hence be moderate. At $Fn >= 0.8$, the differences between resistance results at various separation ratios in the tank tests of Molland et al. (1994a) were very small.

Interference induces cross-flow on the demihulls, which again causes a lift force. The magnitude of the resulting induced drag was investigated by Couser (1996), Couser et al. (1997), and was found to be negligible.

These studies indicate that no demihull interaction effects have a large effect on the resistance of very slender catamarans at Froude numbers between 0.6 and 1.0. We hence do not include any model for demihull interaction.

3.4. Trim and sinkage

Molland et al. (1994a) performed systematic model tests of catamaran hulls of varying demihull geometries, hull separations and Froude numbers, in which trim and sinkage were measured. We have created simplified models for these parameters by linear interpolation in his dataset. The models are parameterized with respect to breadth-to-length ratio, breadth-to-draft ratio, hull separation ratio, and Froude number. The dataset of Molland has been digitized, and linear interpolation is performed between the experimental trim and sinkage values at the tested parameter combinations.

Since all models in the experiments of Molland had relatively low slenderness ratios as compared to that of modern fast ferries, we have extended the dataset by adding vessels of zero breadth-to-length and breadth-to-draft ratios. These are assumed to yield zero trim and sinkage.

Interpolation is performed with the LinearNDInterpolator method of SciPy (The SciPy Project, 2023). This method triangulates the input data using the Quickhull algorithm (Barber et al., 1996), and performs linear barycentric interpolation within each triangle. The trim and sinkage are found through four-dimensional interpolation, as functions of the B/L_{WL}, B/T, and S/L_{WL} ratios, and the Froude number. Here, B and T denote the maximum width and draft of each demihull, and S denotes the separation between demihull centers, respectively.

3.5. Air resistance

Molland and Barbeau (2003) performed a systematic study of the air resistance of various forms of catamaran superstructures, using a combination of wind tunnel experiments and RANS simulations. They concluded that the air resistance varies significantly between different representative superstructure shapes, by a factor of more than two. They also found that the longitudinal air resistance was greater at 15° incidence than with inflow coming directly from the bow, indicating that oblique winds might have large effects on the resistance. Vertical lift forces from aerodynamics were found to be negligible.

Blendermann (1996) performed wind tunnel experiments on the drag of ship superstructures and similar shapes. A trend of increased longitudinal drag at increased incidence, up to approximately 20° relative wind angle, was found. The relative change of longitudinal drag with the incoming wind angle was however found to have a lower magnitude than that observed by Molland and Barbeau (2003).

The superstructures of modern passenger fast ferries can typically be approximated as a box shape on two slender hulls. This resembles closely one of the models tested by Molland and Barbeau (2003), for

which the drag coefficient in headwind was $C_{D,A} = 0.88$. $C_{D,A}$ is defined in Eq. (16), in which D_A, ρ_A, U_A, and A_F denote the air resistance, air density, the relative speed between the vessel and the air, and the projected frontal area of the vessel above water, respectively. Blendermann (1996) measured a very similar value for box shapes of length-width ratios of 2.0–4.0, a range which is relevant to the superstructures of most modern fast ferries. This also corresponds well to the value of $C_{D,A} = 0.86$ for a square-edged trailer truck reported by Hoerner (1965). Molland and Barbeau (2003) showed that the air drag of a catamaran with a box-shaped superstructure fell by 13%–18% when introducing slender hulls under the superstructure, with a height equal to 0.6 times the superstructure height.

$$C_{D,A} = \frac{D_A}{0.5\rho_A U_A^2 A_F} \tag{16}$$

In this first version of our resistance estimation tool, we choose to use the air resistance data for boxes of a length-width ratio of 4.0 from Blendermann (1996), downscaled by 15% to account for the presence of narrow demihulls. We use the full curve of values for the longitudinal air resistance coefficient as a function of the relative wind angle, allowing analyses of oblique winds. The applied drag values are representative of a box-shaped geometry with no fillets on the corners, indicating that it might over-predict the air resistance of fast ferries with sloped front walls or rounded corners. On the other hand, it does not account for the resistance on railings, masts, and instrumentation protruding from the upper deck and the top of the wheelhouse, likely cancelling some of the over-prediction effects from the assumption of sharp corners. This approach implicitly assumes an equivalent reduction of wind drag due to the presence of narrow demihulls at all relative wind angles. This is obviously imperfect, as the reduction of the effective cross-sectional area due to the tunnel opening between the hulls will be dependent on the wind angle. It is however a simplification made in lack of better alternatives.

Wind resistance is affected by the boundary layer near the water surface. As a starting point, we have implemented a correction factor of 0.8 to air and wind resistance, as recommended by Molland and Barbeau (2003).

It should be noted that the air resistance can be highly dependent on geometrical details. Molland and Barbeau (2003) showed that the air resistance of a catamaran could be reduced by approximately 25% by simply tilting the front wall backwards by 50°. Furthermore, slight rounding of the sharp corners reduced the resistance of the truck presented by Hoerner (1965) by 36%. Hoerner reported the air drag coefficient of two different merchant ships as $C_{D,A} = 0.68$ and $C_{D,A} = 1.22$, differing by a factor of 1.8. The wind resistance formula by Isherwood (1972) predicts wind resistance coefficients of $0.30 \leq C_{D,A} \leq 0.40$ if inputting approximate geometrical numbers for fast ferries. This was however based on geometries of merchant ships. Oura and Ikeda (2008) reported $C_{D,A} \approx 0.45$ in headwind for an Incat 112 m wave-piercing catamaran. The superstructure was faired and relatively different from the smaller type of passenger-only catamarans dealt with herein. The sensitivity to geometrical details, as well as the large variation in the reported wind resistance coefficients in published literature, calls for caution in the use of our standard values of wind resistance. However, we believe they are representative of modern fast ferries of which the superstructure is relatively square in nature.

3.6. Added resistance from wind

The procedure of Section 3.5 can be used directly to quantify the added resistance due to wind. We only account for the direct effect of wind on the longitudinal forces, and neglect secondary effects from steering losses or side force-induced hull resistance. Experiments by Molland and Lee (1997) indicate that the side force produced by an angle of attack on demihulls is 1.4–2.0 times higher than that estimated by low-aspect-ratio lifting surface theory (Faltinsen, 2005). Significant variation with Fn is observed. This prevents the creation of a simple model for the induced drag as a function of side force due to wind.

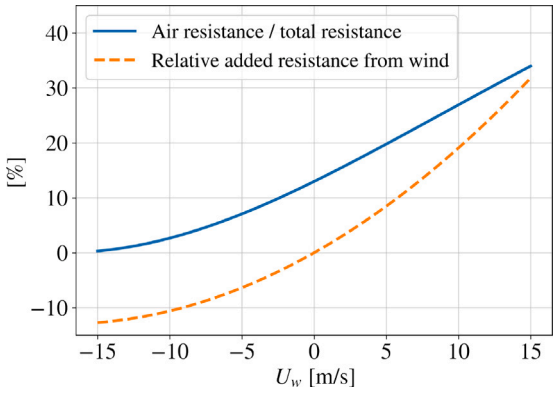

Fig. 8. Aerodynamic resistance and the relative added resistance from wind, for a 40 m fast ferry in longitudinal winds operating at 17.5 m/s. Positive U_W indicates headwinds.

To estimate the error that is made from neglecting induced drag due to aerodynamically induced side force, we use the assumptions and case vessel from Section 3.5. With a 20 m/s side wind, this experiences a relative wind angle of 48° and $C_{Y,A} = 0.75$. $C_{Y,A}$ is defined in Eq. (17), in which $F_{Y,A}$ and A_L denote the aerodynamic force in the transverse direction and the projected lateral area of the vessel above water, respectively. With values from Couser et al. (1997) at $Fn = 0.35$ and $Fn = 1.0$, we find that this creates drift angles of 2.5° and 1.8°, respectively. The added resistance from the resulting induced drag constitutes 0.25% and 0.19% of the transit power for the two speeds. This indicates that no significant error is made from neglecting the hydrodynamics-induced drag due to the wind-induced side force.

$$C_{Y,A} = \frac{F_{Y,A}}{0.5\rho_A U_A^2 A_L} \tag{17}$$

We find it interesting to include a case study on the relative importance of air and wind resistance. To study this, we evaluate the modern passenger fast ferry MS Tyrhaug, for which open data on dimensions and machinery are available (Brødrene, 2022b). We assume the average height of the superstructure to be equal to its width, the propulsive efficiency to be 70%, and the relative load at service speed to be 80% of the maximum continuous rating of the engines. This allows a resistance estimate at its service speed of 34 knots, and a comparison with the aerodynamic resistance. Fig. 8 shows the added resistance due to wind, and the ratio of the aerodynamic resistance to the total resistance. All results are for a vessel speed of 34 knots = 17.5 m/s operating in headwinds or tailwinds, with positive wind speed values indicating headwinds. U_W denotes the wind speed.

Several interesting observations can be made from Fig. 8. Firstly, the air resistance at zero wind constitutes 13% of the total resistance, slightly exceeding the typical range for fast catamarans stated by Molland and Barbeau (2003). This indicates that aerodynamic improvements are indeed a topic worth pursuing, especially in the setting of transitioning to zero-emission energy carriers for which an increased energy requirement comes at a high financial cost and a significant weight penalty, further increasing the energy requirement.

The magnitude of the added resistance due to wind is worth noting. In headwinds of 10 m/s and 15 m/s, which are within normal operating conditions in wave-sheltered regions, the resistance increases by 19% and 32%, respectively. This can have significant implications for energy costs and transit times of conventional vessels. For battery-powered vessels with recharging between each transit, this might also imply that significant reserve power and energy storage must be available.

3.7. Added resistance from waves

Added resistance from waves is created by wave reflection and wave radiation connected with ship motions. The former effect is dominating for short waves (Faltinsen, 1990), and can be estimated by formulae presented by Faltinsen et al. (1980). With the assumptions presented for MS Tyrhaug in Section 3.6, and an assumption of a maximum wave steepness of $H/\lambda = 1/7$ and a maximum wave height of 2.0 m, we can estimate the wave-length dependent values of the added resistance due to reflected waves in head seas. This yields a maximum added resistance of 1.7%, indicating that we can safely neglect this effect.

Radiation of ship-generated waves creates the largest contributions to added resistance (Faltinsen, 1990), and has a significant effect when $1 \leq \lambda/L \leq 1.75$ (Faltinsen, 1990, 2005; Vernengo et al., 2021; Doğrul et al., 2021). λ denotes wave length. Passenger-carrying fast ferries typically operate in sheltered waters where long ocean waves are not present. Carter (1982) gives formulae for estimating the significant wave height $H_{1/3}$ and the spectral maximum period T_0 for fetch-limited seas, given here as Eqs. (18) and (19), respectively. f denotes the fetch distance in kilometres (km) and U_{10} denotes the wind speed in meters per second (m/s) 10 meters above the water surface. The corresponding length of a deep-water wave can be found from the dispersion relation $\omega^2 = kg$ (Faltinsen, 1990), where ω is the wave frequency in rad/s and $k = 2\pi/\lambda$. For a typical fetch distance of 15 km and a wind speed of 10 m/s, this yields a peak of wave energy at a wave length of 16 m. It is evident that this is below the wave length interval for which the added resistance due to ship motions has a significant effect, at least for the majority of modern passenger fast ferries.

$$H_{1/3} = 0.0163 f^{1/2} U_{10} \tag{18}$$

$$T_0 = 0.566 f^{3/10} U_{10}^{2/5} \tag{19}$$

Vernengo et al. (2021) studied the added resistance in waves of slender catamarans using a Rankine source-based Boundary Element Method (BEM). Investigating irregular seas of different peak periods, the highest observed value of the mean added resistance coefficient $\bar{\sigma} = \bar{R_{AW}}/(\rho g \zeta^2 B^2/L)$ was 1.0. R_{AW}, ζ, and B_d denote the added resistance in waves, wave amplitude, and width, respectively. This was for the highest studied Fn of 0.6. Doğrul et al. (2021) studied a slender catamaran at $Fn = 0.35$ in regular waves in the range $0.7 \leq \lambda/L \leq 1.8$, reporting a peak of the mean added resistance coefficient to be 2.5. The slenderness ratio of both vessels was significantly lower than that of modern fast ferries. Using the value of 2.5 and the assumptions for MS Tyrhaug from Section 3.6, we find that the mean added resistance due to radiated waves constitutes less than 1.5% and 6% of the calm-water resistance if operating in 1 m and 2 m significant wave heights, respectively.

Vernengo et al. (2021) shows that the peak of the added resistance appears at $\lambda/L \approx 1.5$, coinciding with peaks of the heave and pitch transfer functions. The former obtains a value of 2.5, indicating that 2.5 m heave oscillations would be present in a 1.0 m regular-waves condition. It is quite certain that the shipmaster would either reduce speed or change course in the case of such motions in a passenger-carrying craft, avoiding the situations of peaks in added resistance due to radiated wave energy.

Further support for added resistance being of secondary importance can be found in a study by Faltinsen et al. (1991), where vertical accelerations and speed loss of a slender catamaran were studied through a range of wave lengths and wave periods. Only in one of the 23 studied cases was the standard deviation of vertical accelerations below the limiting criteria for transit passengers (NORDFORSK, 1987), and in that case the involuntary speed loss was a mere 1.8%.

To sum up, published literature indicates that wave lengths which create significant added resistance from waves are unlikely in typical operation regions of fast ferries, and if they would occur it is likely that the shipmaster would reduce speed or change course due to large ship motions. Even if the latter did not happen, the effects on resistance would be small. We hence omit any modeling of added resistance in waves in the current resistance model. This limitation must be borne in mind if using the model to assess resistance in non-sheltered waters.

The model presented herein is intended for use with known speed data, e.g. from AIS, capturing voluntary and involuntary speed loss. Based on the above, it is judged likely that the effect on resistance from reduced speed in waves is significantly larger than that from added resistance in waves.

3.8. Other resistance components

Resistance from current might be significant since it increases the relative velocity between hull and water. This can be included by simply adjusting the forward speed used in the resistance model.

Spray resistance has not been included. Couser et al. (1997) argues this is of little importance for total hydrodynamic resistance estimates.

Resistance from appendages is not included. This is assumed to be included in propulsive efficiency when estimating the power requirement.

3.9. Implementation

The resistance calculation software is written in Python and consists of two main components; A pre-processor and a live resistance estimation processor.

Pre-processing consists of four steps. It takes input in the form of Wavefront files (.obj), splitting the hull into a desired number of longitudinal strips. The properties of the strips are calculated at various submergences and stored in arrays. Linear interpolation functions are then created, relating strip and transom properties to the local draft. Examples of such properties are the wetted surface, the B/T ratio and the maximum width of the strips, which are needed in calculations of the frictional resistance, added mass and wavemaking resistance, respectively. Added mass coefficients are imported from a database and interpolation functions are created, relating it to geometrical strip properties. The creation of interpolation functions for strip properties in a pre-processing step means that no mesh processing is needed when estimating the resistance, speeding up the calculations significantly.

The live resistance processor takes a wave field model as well as six-degree-of-freedom (six-DOF) vectors of the global position, velocity, and acceleration of the hull as input. It then calculates the local relative water velocities, accelerations, and water levels at each strip, finds the added mass, the wetted surface, and other relevant parameters from interpolation functions, and calculates the stripwise forces based on the theory presented herein. A downstream extension of the hull is created to account for the wake hollow in the wavemaking resistance calculation. Forces are finally summed into a six-DOF force vector.

The resistance estimates comprise frictional forces, wavemaking drag, transom-stern pressure loss, and air and wind resistance. The presented submodels for form factors and the shape of the wake hollow are used in the calculations of frictional forces and the wavemaking drag, respectively. Trim and sinkage can either be specified, or the presented submodel can be used for setting these states.

The execution time of the resistance processor on an Intel® i7-10875H CPU is in the order of seconds for a full-scale resistance simulation, despite the absence of parallelization or compiling of any part of the code. Comparatively, the RANS simulations herein required processing resources in the order of 10^3 CPU hours on a simulation cluster based on AMD EPYC 7543 processors.

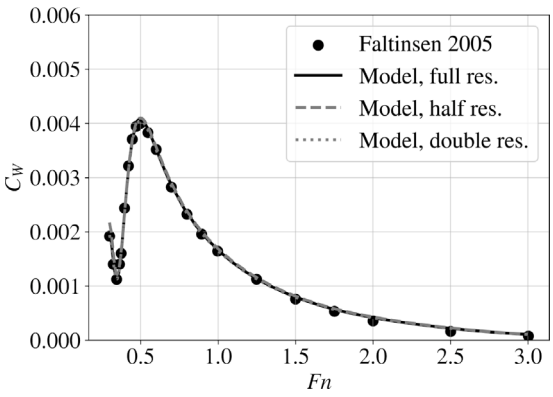

Fig. 9. Wavemaking resistance as predicted by Faltinsen (2005) and the current model at final, halved, and doubled numerical resolutions.

Table 3
Main settings of RANS simulations. More details are given in Appendix B.

Parameter	Value
Turbulence model	$k-\omega$ shear stress transport (SST)
Two-phase model	Volume of Fluid
Re	Equal to experiment
y^+	40
No. prism layers	4
Domain depth	Equal to experiment

4. Verification

The implementation of Michell's thin ship theory involves a relatively large amount of code, including geometry mesh handling, splitting into strips, a series of interpolation steps, and the implementation of the theory presented by Tuck (1987). It is deemed reasonable to perform a verification of this part of the resistance model, and to check its results for dependency on the numerical resolution. We do this by comparing results to those presented by Faltinsen (2005), for thin-ship calculations of the wavemaking resistance of a Wigley hull (Wigley, 1942). The length, width, and draft of the hull were 8 m, 0.75 m, and 0.5 m, respectively, and it was operated at $0.3 \leq Fn \leq 3.0$.

Fig. 9 shows wavemaking resistance predictions from Faltinsen (2005) together with those of the presented resistance model. After experimenting with the numerical resolution, we have identified a setup for which the results are not affected by further refinement. These are 200 strips, 200 wave radiation angles, vertical integration over 201 waterlines, and the latter being done by linear interpolation of hull data at 40 waterlines. The figure includes results using those settings, as well as results created with halved and doubled resolutions in all four numerical dimensions. There is practically no difference between these, and all agree very well with the data of Faltinsen (2005). All model-scale resistance simulations herein were performed with these settings. In the full-scale simulations in Section 5.2, the number of wave radiation angles was doubled to reduce noise in the wavemaking resistance predictions.

5. Validation

Our validation study has two aims. We start by investigating the accuracy of the presented resistance model for typical fast ferry hulls, including reduced-draft operation. The latter is relevant if using the model to analyze foil-supported vessels. Finally, we study the correspondence between the resistance data from a towing tank test of a modern commercial fast ferry, to resistance predictions made with a combination of the hull geometry and resistance models presented herein. This last step is performed to evaluate whether this combination of models can be used for estimating the power requirement of existing vessels, based on knowledge of only a few design parameters.

5.1. Validation of the resistance model

5.1.1. Method

The aim of the first validation step is to investigate the accuracy of the presented resistance model when used on hulls resembling those of modern fast ferry catamarans, at design draft and reduced drafts.

Several hull series have been thoroughly studied in the literature, many of which were mentioned in the introduction. Among these, the NPL hull shape, first published by Bailey (1976), stands out as the most representative of a modern fast ferry. More slender varieties, both monohull and catamaran versions, were studied by Insel (1990), Molland et al. (1994a), Molland and Lee (1995), Couser (1996), Molland and Lee (1997), Cyberiad (2015) and Shi et al. (2021). The hull comprises representative features such as rounded bilges, a relatively slender forebody, and a lightly sloped stern profile. There are however some deviations from modern fast ferry designs, such as V-shaped bottoms of the stern sections and significantly lower slenderness ratios. Between the varieties of the hull, the *NPL 4a $S/L = 0.2$* has been most thoroughly studied in recent years (Cyberiad, 2015; Shi et al., 2021). Its main particulars are listed in Table 2. A detailed description of the baseline geometry and scaling procedures for different slenderness ratios were given by Bailey (1976) and Molland et al. (1994a), respectively.

The *NPL 4a, $S/L = 0.2$* hull constitutes a challenging case for the resistance model since the hull has a far lower slenderness ratio than that of modern fast ferries. This yields a limiting case for the validity range of the thin-ship wave resistance calculation model. It also leads to significant wave field interaction effects in the between-hull tunnel, which are not modeled. We hence do not expect perfect correspondence between the experimental data and model predictions for this hull.

Published data on the NPL hull does not include reduced-draft operation, and the hull form deviates from that of modern fast ferries in several ways. Furthermore, as we shall discuss below, high-Froude-number towing tank data on its resistance might be affected by finite-depth effects. We therefore generate new resistance data by RANS simulations of a more slender hull in deep water, at design draft and reduced-draft operation. The geometry is generated with the presented hull geometry model. Simulations are performed with OpenFOAM, and the main settings are outlined in Table 3. More details on the RANS setup are given in Appendix B. To ensure accurate RANS results, we perform RANS simulations of the *NPL 4a, $S/L = 0.2$* hull and compare these with experimental data and previously published RANS results on the same hull. A scripted setup method is used, ensuring consistent settings between those for the NPL hull and the new hull shape.

Much of the validation, specifically all which deals with catamarans of slenderness ratios which are typical for modern fast ferries as well as all reduced-draft cases, is done by comparing the resistance model results with RANS simulation results. We still use the term validation rather than verification for this comparison. This is because we are comparing two simulation approaches which are fundamentally different, and hence do not solve the same theoretical problem. RANS simulations solve the flow physics on a much more detailed level, without many of the simplifications in the resistance model, and are hence expected to be orders of magnitude more accurate than the latter. In the lack of high-quality experimental data on representative hull shapes of known and openly available geometry, we believe this is a reasonable way of validating the presented model.

The new hull form is generated with the hull geometry model, and its main parameters are given in Table 2. Geometry files can be found on the FASTSHIPS website (Godø and Steen, 2023). The hull shape resulted from tuning to fit the geometry to images and other available data for modern fast ferries. Details on the procedure are given in Appendix A. New resistance data is generated at the design draft for Froude numbers ranging from 0.5 to 1.0. Investigation of reduced-draft operation is done for $Fn = 0.8$, from the design draft to 25% of the design draft.

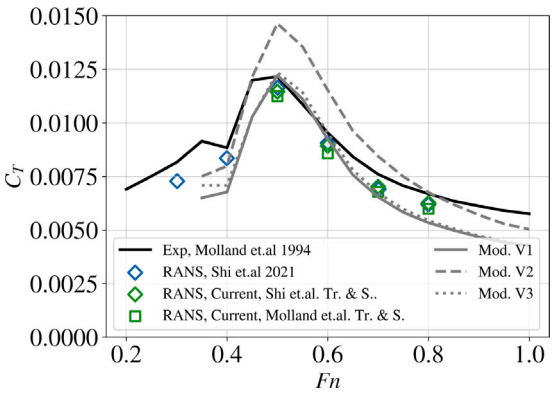

Fig. 10. C_T from experimental data by Molland et al. (1994a), RANS simulations by Shi et al. (2021), current RANS simulations and the resistance model (Mod.).

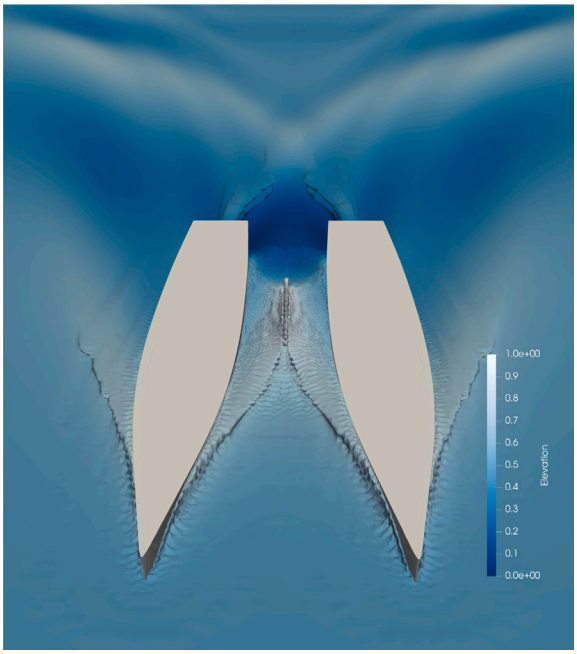

Fig. 11. NPL 4a, S/L = 0.2 at *Fn* = 0.8, trim and sinkage from Shi et al. (2021). Rooster tails curve inwards and a breaking wave is present between the demihulls.

5.1.2. Results and discussion

NPL 4a,S/L = 0.2.

Fig. 10 shows the total resistance coefficient C_T as predicted by the experiments of Molland et al. (1994a), RANS simulations by Shi et al. (2021), current RANS simulations, and the presented resistance model. C_T is conventionally defined as $R_T/(\frac{1}{2}\rho U^2 S)$, where R_T is the total resistance, U denotes forward speed, and S is the wetted surface at standstill. *Fn* denotes the Froude number based on the waterline length at standstill. Two varieties of RANS simulations are included, in which the vessel follows the trim and sinkage values of Molland et al. (1994a) or (Shi et al., 2021). Enforced sinkage is applied at LCB. The domain depth is set equal to that of the experimental campaign of Molland et al. (1994a).

It is seen that the new RANS results correspond very well to those of Shi et al. (2021). The similarity with both the results of Shi et al. (2021) and Molland et al. (1994a) is best when using the trim and sinkage values of the former. All results then deviate less than 2% from those of Shi et al. (2021). The correspondence between our RANS simulations and the experimental data is practically equal to that of the RANS simulations of Shi et al. (2021) and experimental data, and is judged acceptable.

Potential sources of discrepancies between the experiment and RANS include laminar-flow effects due to low Reynolds numbers, flow separation on turbulence stimulation studs, air resistance on the hull attachment system, potential geometrical inaccuracies in the experiment and geometrical inaccuracies in the RANS simulations due to coarse resolution of the hull data of Bailey (1976). The latter is discussed in Appendix C. Additionally, there might be a reduced effect of spray on the simulated frictional drag, as the hull height above water was limited to 0.5 times the draft to save on computational resources.

All simulations with the resistance model were done with trim and sinkage values from Molland et al. (1994a), applied at LCB. To investigate the effect of various transom-stern modeling choices, we include results from three sets of settings, as described in Table 4. There is generally good correspondence between the RANS data and V1 and V3 of the resistance model, particularly for *Fn* >= 0.5. The resistance hump close to *Fn* = 0.5 is well captured, with a trend of a slight under-prediction of resistance in the higher-*Fn* range. The differences between the predicted resistance from the resistance model and the RANS results are generally not much larger than those between RANS results and the experimental data. Version three of the resistance model, denoted V3, differs from version one (V1) only by the fact that the width of the wake hollow does not reduce towards its downstream end. This yields practically the same results as version one. The latter incorporates a parabolic decrease of the wake hollow width towards the downstream end.

Version two of the resistance model (V2) adds a contribution to resistance from the pressure loss at the transom stern, as detailed in Section 3.1.2. The reason this leads to an over-prediction of the resistance is not completely clear. Our main theory is that it is because the resistance model does not account for wave elevation. In the tested range of Froude numbers, the wave trough from the bow wave leads to a significant lowering of the water level surrounding the transom stern, reducing the effective submerged transom area. Adding a resistance component based on zero-wave-elevation submerged area hence over-predicts this contribution to resistance. Neglecting the effect of pressure loss on the transom yields a smaller error than adding it with an over-predicted submerged transom area based on the undisturbed water surface level.

Several reasons might be identified for the under-prediction of resistance at *Fn* = 0.8. The presented resistance model does not take into account the limited tank depth used in the experiments. This was 1.85 m, only slightly more than the waterline length of the model, meaning the high-speed cases approached the critical depth Froude number. The ratio of tank depth to ship length is however well above the limiting criterion of $h/L >\approx 0.4$ for when the effect of the tank bottom on the resistance should be small, according to Faltinsen (2005). Some effects from the limited tank depth on the wavemaking resistance cannot be ruled out, but it is believed to be small.

Inspecting the shape of the free surface, as shown in Fig. 11, shows that this hull yields challenging conditions for a resistance model as simple as that presented. The figure shows the results of the RANS simulation at *Fn* = 0.8, with trim and sinkage according to the values of Shi et al. (2021). A significant wave trough is visible in the tunnel between the demihulls, close to the stern. This is far deeper than outside of the demihulls, indicating strong interference effects. A secondary effect of this is that the rooster tails downstream of the transoms are deflected inwards towards the wave trough. Neither of these effects are captured by the wavemaking resistance theory of Tuck (1987). This implementation of thin-ship theory inherently models a symmetrical flow about each demihull, since only sinks and sources are used on the centreplane. Furthermore, the resistance model cannot capture energy losses connected with the presence of a breaking wave in the tunnel. Nor can it accurately capture the changes of the wetted surface due to wave elevation and spray, although a correction for this is implicitly included in the form factor. The relatively low slenderness ratio of the

Table 4
Simulation settings for simplified model.

	V1	V2	V3
Transom pressure loss correction	Off	On	Off
Wake hollow model	Full	Full	Vertical only

NPL 4a hull means that the effects of unmodeled physics such as spray, wave elevation, and demihull interference are expected to be more significant than in cases with more slender hulls.

Since we do not focus on low-speed operation, we do not dwell much with the fact that relative errors are larger for $Fn \leq 0.4$. A good argument can be made for why this is not a significant problem for estimates of the energy requirement of fast ferries. A typical design *Fn* of such vessels can be found from open data to be approximately 0.8–0.9 (Brødrene, 2022a). If we assume a design *Fn* of 0.85 and approximate the power requirement as a function of U^3, the power requirement at $Fn = 0.4$ is only 10% of that at design speed. Combined with the fact that the vessel likely spends much more time at design speed than at reduced speed, this means that a larger percentage error in C_T at $Fn = 0.4$ likely makes no significant impact on the accuracy of calculations of energy requirement on a route.

NTNU FF1.

The total resistance coefficient for the NTNU FF1 hull, as predicted by RANS and the presented resistance model, is shown in Fig. 12. Three sets of modeling settings are again included, as described by Table 4. The RANS simulations were run with free trim and sinkage at 1:25 scale. Scaling was done to achieve a similar Reynolds number and hence similar mesh layering settings as in the simulations of the NPL 4a S/L = 2 hull. Trim and sinkage values from RANS were used in all resistance model simulations, except for the simulation termed *V1_NoTr.& Sink* where the trim and sinkage were set to zero. It is seen that V1 and V3 of the model predict both the trends and absolute values of C_T well through the whole range of *Fn*. This is particularly so for *Fn* >= 0.7. V2 consistently over-predicts the resistance, indicating that the inclusion of the base drag model does not improve accuracy in the current case. The error in dimensionless form is reduced with increasing *Fn*, a phenomenon which is connected with the fact that the ventilated-stern base drag is a constant value which is independent of speed.

Interestingly, the results from $V1_{NoTr.\&Sink.}$ correspond better with the RANS results than any other simulation data set. A possible explanation is that trim and sinkage mainly occur as a result of pressure forces connected with hull wave-making, partly cancelling the relative change of water levels along the hull due to positive and negative wave elevation in the forward and aft parts, respectively. Since the form factors were calculated based on simulations without trim and sinkage, and the frictional resistance coefficient used in its calculation was made dimensionless with respect to the wetted surface at standstill, they implicitly correct the calculation of frictional resistance for dynamic wave elevation in cases without trim and sinkage. Similarly, the wake hollow model was created from simulations without dynamic trim and sinkage. Combining these models with setting the trim and sinkage to zero might effectively simplify the physics in two ways, from which the errors partly cancel. If, conversely, using the trim and sinkage prediction model, without also correcting for the local wave elevation, we effectively apply a correction to the wetted surface and the submergence of the transom relative to that used when finding the form factors and creating the wake hollow model.

Fig. 13 presents a resistance breakdown for the NTNU FF1 hull geometry, splitting the resistance into pressure and frictional components. The results from RANS and version one of the simplified model with zero trim and sinkage are compared. It is seen that the simplified model captures the trends and absolute values of both pressure resistance and frictional resistance very well. A slight under-prediction of both

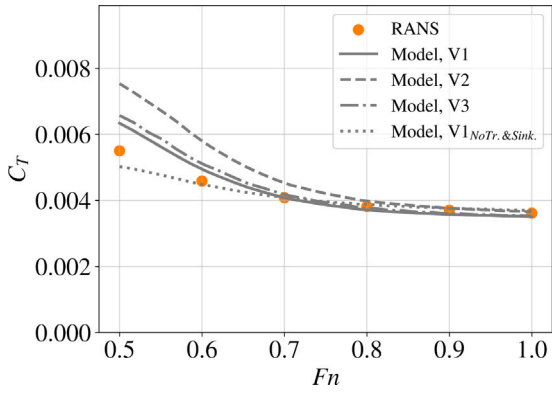

Fig. 12. C_T of the NTNU FF1 from RANS simulations and the presented resistance model. V1, V2, and V3 as described in Table 4. "*NoTr.&Sink.*" means zero trim and sinkage.

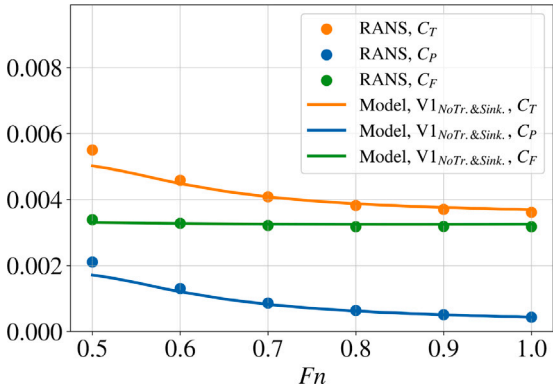

Fig. 13. Resistance breakdown for the NTNU FF1, from RANS simulations and the presented resistance model. "*NoTr.&Sink.*" means zero trim and sinkage.

pressure resistance and frictional resistance is done at $Fn = 0.5$. This is typically the *Fn* where the wavemaking drag coefficient peaks and the wave elevation is at its most significant. The neglect of trim and sinkage is also a significant simplification for this operating condition. In light of this, the magnitude of the errors is surprisingly small. For all other *Fn*, the correspondence with RANS is very good. The fact that the resistance model predicts wavemaking and frictional resistance coefficients correctly indicates an ability to capture the effects of varying slenderness ratio, as this will have opposite effects on these resistance components.

The total resistance coefficient for the NTNU FF1 hull for varying drafts, as predicted by the model and RANS simulations, is shown in Fig. 14. T and T_d denote draft and design draft, respectively. The drag coefficients were nondimensionalized with respect to the wetted surface at the design draft. It is seen that the correspondence between the resistance model and RANS simulations is very good for $T >= 0.5T_d$. At further draft reductions, the accuracy is still acceptable for engineering purposes. The change of slope of C_T relative to T/T_d at $T/T_d \approx 0.5$ coincides with the emergence of the transom and aft ship bilges. At further draft reductions, the wetted surface and hence resistance reduces rapidly, since near-horizontal parts of the hull are emerging from the water. This effect is qualitatively captured by the resistance model, although the accuracy decreases as the draft is further reduced beyond this point. This likely originates from the lack of accounting for variations in the wetted surface due to the wave pattern of the hull, a simplification from which the errors will be greatly increased due to near-horizontal hull surfaces protruding from the water surface at shallow drafts. It is worth noting that, in analyses of foil-supported hulls or hydrofoil vessels during take-off, the relative

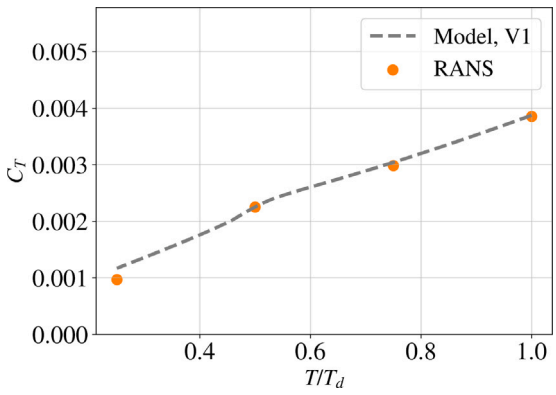

Fig. 14. C_T of the NTNU FF1 hull at reduced-draft operation, as predicted by version 1 of the resistance model (Mod. V1) and RANS simulations. V1 as described in Table 4.

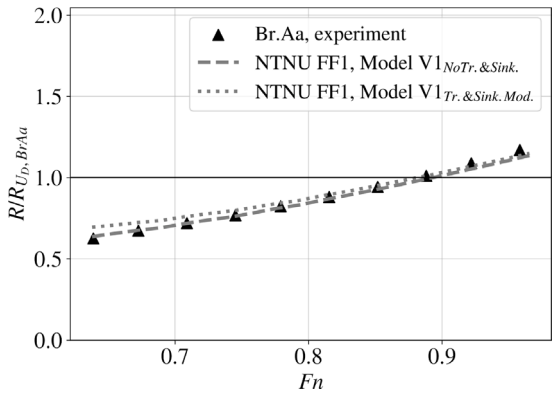

Fig. 15. Resistance curves from experimental data for a Brødrene Aa vessel and resistance model predictions for the NTNU FF1 at equal length and displacement.

error in the total resistance will be reduced due to a gradually smaller relative contribution from hull drag as the draft is reduced.

5.2. Validation of the combined hull and resistance models

5.2.1. Method

In this section, we investigate whether a set of geometry parameters can be specified for the presented hull geometry model so that the predicted resistance of the resulting hull by the resistance model corresponds to that of a modern fast ferry. We choose to use the NTNU FF1 geometry, with parameters as presented in Table 2. This hull shape was specifically tuned to fit openly available data and images of the hull shapes of modern fast ferries, as described in Appendix A.

Resistance predictions are compared to towing tank data provided by the shipyard Brødrene Aa, for a 275-passenger fast ferry operating in a Froude number range of 0.62 to 0.95. The vessel is less than 10 years old and currently operates a Norwegian public route. The waterline length is set equal between the NTNU FF1 and Brødrene Aa hulls, and the draft of the former is adjusted to give equal displacement to that in the tank tests of the latter.

The experimental model had zero trim at standstill and was free in trim and sinkage. We have not gained access to dynamic trim and sinkage data. We include two versions of resistance estimates from the simplified model, namely with trim and sinkage forced to zero and with both predicted by the presented trim and sinkage model.

5.2.2. Results and discussion

Fig. 15 shows the resistance curves for the Brødrene Aa and NTNU FF1 vessels. Subscripts *No Tr. & Sink* and *Tr. & Sink Mod.* denote results with trim and sinkage forced to zero and with trim and sinkage predicted by the presented model, respectively. For confidentiality reasons, all resistance data is given relative to that of the Brødrene Aa vessel at design speed, denoted $R_{U_D,BrAa}$. It is seen that the correspondence with the experimental data is good for both sets of results. A slightly closer resemblance to the experimental data at lower Froude numbers is seen from simulations with zero trim and sinkage. Results from both models match the experimental data very well when operating close to the design speed.

These results indicate that, with known data for length and displacement, the NTNU FF1 hull can be used together with the presented resistance model to yield relatively accurate resistance predictions for modern fast ferries. The geometry can be generated by the open-source FASTSHIPS Hull Generator software or downloaded from its companion website (Godø and Steen, 2023).

6. Conclusions

This paper has presented a comprehensive two-part method for calculating the resistance of modern passenger fast ferries. The method consists of a hull generation model and a resistance calculation model. The hull generation model enables the creation of realistic fast ferry demihulls based on a simple set of inputs, and its accuracy has been verified through a thorough validation study. The resistance calculation model has been shown to accurately predict the resistance of slender catamarans, both at design draft and during reduced-draft operation.

The novel contributions of this study encompass both modeling and validation efforts. Within the former, the hull generation model offers an efficient way of creating representative geometries suitable for the analysis and optimization of slender catamaran fast ferries. To facilitate its future use, we have made the code openly available under an open-source license (Godø and Steen, 2023).

The resistance calculation model combines established methods with novel modifications to such. One of the modifications is a proposed model for the “wake hollow” downstream of submerged transom sterns, accompanied by a systematic investigation of its accuracy across different speeds and geometries. Another modification addresses the form factors for slender catamarans, contributing to the ongoing discussion in the existing literature (Molland et al., 1994a; Couser, 1996; Couser et al., 1997; Armstrong, 2000). Our study presents new results based on a modern friction line, established through a systematic set of 3D Reynolds-Averaged Navier–Stokes (RANS) simulations involving various submerged geometries and a range of Froude numbers. A model is created, based on an empirical fit to the data.

The validation efforts comprise a series of evaluations to assess the ability of the proposed modeling approach to predict the resistance of modern fast ferry hulls. The assessments include a detailed analysis of resistance predictions across different Froude numbers and operating drafts. Furthermore, through comparison with experimental data, we have demonstrated that the application of the resistance model on a hull generated with the hull model allows accurate resistance predictions for a modern fast ferry across a wide range of Froude numbers. This indicates that our tools can be used for calculating the resistance and energy requirement of modern fast ferries with minimal information on the vessel.

It should be noted that while the resistance model has been validated against experimental data and 3D RANS simulation results for two different hullforms and various drafts, its accuracy cannot be guaranteed for cases with significantly different geometrical features. Furthermore, caution should be exercised if employing the model outside the Froude number ranges investigated in this study.

Future research should investigate the validity limits of the resistance model with respect to the slenderness ratio of the hulls. Additionally, if analyzing operations in rough weather conditions and unsheltered waters, the topic of added resistance when operating in long waves should be further investigated, and relevant additions to the

model should be considered. Additionally, it is noted that the presented version of the wake hollow model depends on the absolute ship speed U to the power of 2/3. Further investigation into the possibility of rendering this model dimensionless could add significant value to the model.

The hull generator and resistance calculation models have been implemented as modules in the FASTSHIPS (Fast and Simple Tool for Simulation of HIgh Performance Ships) software package, developed by the Department of Marine Technology at the Norwegian University of Science and Technology (NTNU) (Godø and Steen, 2023). This work serves as documentation, testing, and validation of the software. In the future, the software will be utilized to assess the technical feasibility and optimal design of zero-emission fast ferries on existing routes. Thanks to their numerical efficiency, our models allow for simulations of high-fidelity operational profiles and assessments of a wide variety of hull shapes, fostering creative efforts in addressing the zero-emission challenges of future fast ferry design. Furthermore, the accurate resistance predictions at reduced drafts indicate that the resistance model can be combined with hydrofoil models to assess hydrofoil-assisted hulls or analyze and optimize the take-off phase of hydrofoiling fast ferries.

CRediT authorship contribution statement

John Martin Kleven Godø: Conceptualization, Methodology, Software, Formal analysis, Investigation, Writing – original draft, Visualization. **Sverre Steen:** Conceptualization, Supervision, Writing – review & editing, Project administration, Funding acquisition, Resources. **Odd Magnus Faltinsen:** Methodology, Writing – review & editing.

Declaration of competing interest

The authors declare that they have no known competing financial interests or personal relationships that could have appeared to influence the work reported in this paper.

Data availability

An implementation of the presented hull geometry model and the NTNU FF1 hull geometry are shared on https://www.ntnu.edu/imt/software/fastships.

Declaration of Generative AI and AI-assisted technologies in the writing process

During the preparation of this work the authors used the language model ChatGPT by OpenAI in order to improve the spelling, language and grammar of this paper. After using this tool/service, the authors reviewed and edited the content as needed and take full responsibility for the content of the publication.

Acknowledgments

The presented work was financed by the *enabling Zero Emission passenger Vessel Services* (ZEVS) project (NFR grant No. 320659) and SFI Smart Maritime (NFR grant No. 237917). RANS simulations were partly performed on Uninett Sigma2 national high-performance computing resources as part of project NN9389K.

Appendix A. NTNU FF1 hull details

The NTNU Fast Ferry 1 hull, hereafter abbreviated NTNU FF1, is a subset of the presented hull geometry model which has been designed to represent, to the level of detail possible from open data, the hull of a modern fast ferry. Available images of modern vessels from the Brødrene Aa and Oma Baatbyggeri shipyards, on land and in water, have been used in combination with data on their main dimensions published on the respective shipbuilders' websites, to establish approximate ratios of length/draft ratios, draft/width ratios, the relative submergence of the transom stern, and the hull separation ratio. These have also been used in visual tuning of the longitudinal distributions of the width and draft. Our own pictures of modern fast ferries, taken from publicly available spaces in Trondheim, have also been used. In cases where significant differences were found between the hull shapes of the mentioned yards, we have chosen to approximate the one of Brødrene Aa. The reasoning behind this is that this company is the most active supplier of newbuilds in the Norwegian fast ferry market, while also being an exporter of vessels to foreign markets.

The main parameters of the resulting hull shape are given in Table 2. It is evident that our approach leads to a hull of a very high slenderness ratio. No public data on the displacement of modern passenger fast ferries has been found, allowing a direct confirmation of this number. However, conversations with designers have revealed that our slenderness ratio is relatively representative. The NTNU FF1 was generated with FASTSHIPS v1.0.0, and its full geometry can be found online (Godø and Steen, 2023).

Appendix B. RANS setup

All RANS simulations herein were conducted using OpenFOAM v 2112, with meshes generated by snappyHexMesh. We used the interFoam solver and the PIMPLE solution algorithm with 3 outer and 2 inner correctors. All simulations were multiphase, modeling air and water, using Volume of Fluid (VoF) interface capturing. Adjustable time steps were applied, limiting the Courant numbers generally to 15 and to 10 in the interface region. Turbulence modeling was done with the SST (Shear Stress Transport) k-ω model and wall functions. Discretization was done with the linear upwind scheme for convective terms of the momentum equation and the Euler scheme in time. All other applied schemes were second-order accurate. For reproducibility, the key OpenFOAM dictionaries that were used when simulating the NTNU FF1 at Fn = 0.9 in model scale have been uploaded to the companion website of the FASTSHIPS software package (Godø and Steen, 2023).

The domain modeled half the vessel, with a symmetry plane between the demihulls. In simulations of the NTNU FF1 hull, we used sideways, downwards, upstream, and downstream domain extents of 2, 2, 2, and 20 ship lengths, respectively. A fixed-value flow speed was prescribed on the upstream, side, and bottom boundaries and a zero pressure gradient was prescribed on the downstream boundary. Simulations of the NPL 4a hull were performed with the same settings, except that the domain depth of the experiments of Molland et al. (1994a) was replicated, and a symmetry plane was used on the tank bottom boundary. A prism-layer mesh was used near the hull, with a target y^+ of 40 based on the friction line of Eça and Hoekstra (2008). The cell sizes varied through the remainder of the domain, with refinements near the hull, downstream of the transom and near the free surface. In the standard settings used when producing all results of Section 5, the near-hull cell size was 0.21% LWL outside the prism layer. Five prism layers were applied. Prism layers were not applied to the air-exposed deck, and the mesh was here only refined to a cell size of 0.83% LWL. Near the free surface, the cell size in the horizontal directions equaled 1.67% LWL and the vertical cell size was 0.21% LWL. A between-demihull refinement zone of cell size 0.21% LWL stretched horizontally from $0.3 \times LWL$ to $1.1 \times LWL$ from the bow and vertically from $-1 \times T$ to $1 \times T$. Transition regions between the refinement zones were sized so that there were always at least 3 cells of equal sizes between refinement levels. The resulting meshes counted approximately 7.6 million cells for the NTNU FF1 simulations and 8.1 million for the NPL 4a simulations.

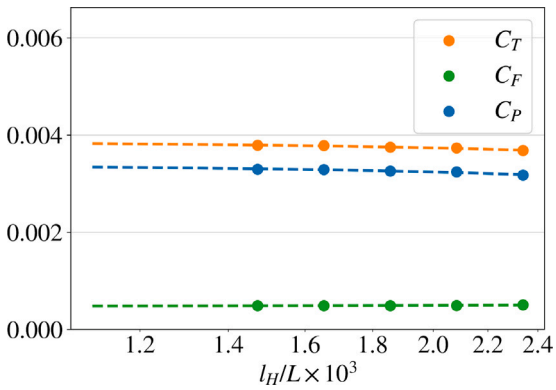

Fig. B.1. Convergence of the resistance coefficients as a function of the numerical resolution. l_H denotes the near-hull cell size outside the prism layer.

B.1. Numerical uncertainty in the RANS simulations

The numerical uncertainty was assessed by the Richardson Extrapolation technique, as described by 28th ITTC Resistance Committee (2017b). This was done for the NTNU FF1 hull at Fn = 0.9. Meshes of different refinement levels were made by scaling all cell sizes outside the prism layer. y^+ was kept constant and the number of prism layers was varied between four and six to ensure a minimum of variation of the prism-layer growth rates. The latter varied from 1.21 to 1.28. Cell counts spanned from 5.8 million to 18.6 million.

The convergence of the results as a function of cell size is presented in Fig. B.1, where l_H denotes the cell dimension outside the prism layer in the near-hull region. The procedure was repeated for C_T, C_F, and C_P, which denote the total, frictional, and pressure resistance coefficients, respectively. Monotonic convergence was identified for all cases. The simulation resolution used in Section 5 corresponds to $l_H = 0.0021LWL$, indicating 4.8%, 4.8%, and 6.1% uncertainties in RANS predictions of C_T, C_F, and C_P, respectively.

Appendix C. NPL hull details

The NPL hull geometry was described by Bailey (1976). He gave a combination of point offsets, i.e. lateral distances from the centreplane, and a longitudinal distribution of profile heights as measured from the baseline. Some assumptions need to be made in order to create a three-dimensional closed hull from the data, and the ones made in the current work are as follows:

- The geometry description ends at station 10, i.e. the forward perpendicular. We have created a bow shape forward of this station by spline extrapolation to a virtual station 10.2
- Spline interpolation has been used at each station, in order to upsample the number of data points.
- Longitudinal spline interpolation of offsets and the vertical position of offsets has been made in order to upsample the number of stations.
- Point offsets and profile height data cannot be connected smoothly close to the demihull centreplane, without making some assumptions. We have chosen to create a linear interpolation between the station data and the centreplane data, creating a hard edge along the line of the deepest station offset data. This is close to parallel to the longitudinal direction of the hull, and likely has negligible effects on the resistance in the form of local flow separation.

Table D.1
RANS results for the NTNU FF1 at LWL = 1.6 m. Varying *Fn*.

Fn	C_{Tm}	C_{Fm}	k	$x_{z=0.5T_t}$
0.5	0.0045997	0.0032589	−0.053728	0.139
0.6	0.0042116	0.0032426	−0.030961	0.217
0.7	0.0039937	0.0032677	0.000448	0.213
0.8	0.0038540	0.0032690	0.021864	0.220
0.9	0.0037326	0.0032414	0.031886	0.235
1.0	0.0036147	0.0031938	0.033384	0.255

Table D.2
RANS results for the NTNU FF1 at LWL = 1.6 m. Varying draft. T, T_D, and T_t denote the applied, design, and transom drafts, respectively.

T/T_D	T_t	C_{Tm}	C_{Fm}	k	$x_{z=0.5T_t}$
0.75	0.010	0.0035275	0.0031958	0.017376	0.253
0.88	0.015	0.0038142	0.0032155	0.020648	0.240
1.00	0.020	0.0037326	0.0032414	0.031886	0.235
1.12	0.025	0.0036235	0.0032061	0.023636	0.231
1.25	0.030	0.0039765	0.0032755	0.042738	0.225

Table E.1
Key error sources of the resistance model, for the NTNU FF1 operating at *Fn* = 0.9.

Parameter	Base value	Variation	Relative error
$C_{F0}(1+k)$	1.688×10^{-3}	4.8%	3.01%
$C_{D,A}$	0.739	10.0%	1.18%
$\hat{A}$	15.650	10.0%	0.05%
Combined			3.23%
U	3.57	1 kn	4.76%

Appendix D. RANS results

Tables D.1 and D.2 present the RANS results from the studies of form factors and wake hollow length discussed in Section 3. The model-scale wetted surface at the design draft was 0.192422 m^2, not counting the submerged transom. The latter was ventilated in all cases. C_{Tm} and C_{Fm} denote the total and frictional resistance coefficients in model scale, respectively. $x_{z=0.5T_t}$ denotes the longitudinal distance from the transom to the point at which the water surface in the wake hollow has risen halfway back to the undisturbed water surface.

Appendix E. Error analysis of the resistance model

To quantify the sensitivity of the presented resistance model to errors in the input parameters, we present a limited error analysis. This constitutes three steps:

1. Identify key error sources
2. Establish estimates of the uncertainty in each parameter
3. Quantify the effect of parameter uncertainties on resistance predictions

Key error sources are identified as the form factor k_F, the flat plate frictional resistance coefficient C_{F0}, the air drag coefficient $C_{D,A}$, the wake hollow length constant $\hat{A}$ and the forward speed U. In the error analysis, we vary the values of these parameters by ± 10% relative to their base values, except for the form factor k_F and C_{F0}. Re-arranging Eq. (15) yields Eq. (E.1), which directly relates these parameters to C_F. Since we already have an estimate for the uncertainty of C_F from the uncertainty analysis of RANS results in Appendix B, we combine the uncertainties of k and C_{F0} according to Eq. (E.1) and vary this combined parameter by ± this value, i.e. ±4.8%. The key error sources, their base values, and the applied variation are listed in Table E.1. Base values are for the case of the NTNU FF1 hull operating at *Fn* = 0.9.

$$C_{F0}(1+k_F) = C_F \tag{E.1}$$

We assume the errors associated with each error source to be independent of one another. The effect on C_T from varying each parameter is first estimated as $\Delta C_{T,X} = (C^+_{T,X} - C^-_{T,X})/2$. In this equation, X denotes the error source parameter, and the superscripts + and - indicate that the values of C_T are calculated with the parameter X set to its base value scaled by ± the applied variation described above. The total error in C_T is finally predicted as in Eq. (E.2). It is important to note that the error induced by uncertainty in U is not included, as this is not part of the modeling error. The resulting relative error of the total resistance coefficient C_T is 3.23%.

$$\Delta C_T = \sqrt{(\Delta C_{T,C_{F0}(1+k_F)})^2 + (\Delta C_{T,C_{D,A}})^2 + (\Delta C_{T,\hat{A}})^2} \tag{E.2}$$

It is worth investigating the magnitude of the relative error from uncertainty in the forward speed U. Uncertainty in U could for instance originate from using speed data from measurements of speed over ground, which do not take currents into account. To investigate the impact of such errors, we use a current of 1 knot as an example. This is not an uncommon magnitude of current in fjords or in narrow passes in archipelagos. An equivalent analysis to the above, with U varied by ± 1 knot scaled to model scale, yields a relative error of 4.76%. The predicted uncertainty of the resistance model is hence within the likely uncertainty which uncertain speed measurements may impose.

References

26th ITTC Propulsion Committee, 2011. ITTC - Recommended Procedures and Guidelines, 1978 ITTC Performance Prediction Method, Revision 2. techreport, International Towing Tank Conference, Revision 2.

28th ITTC Resistance Committee, 2017a. ITTC Quality System Manual, Recommended Procedures and Guidelines, Procedure Resistance Test. Technical Report, International Towing Tank Conference.

28th ITTC Resistance Committee, 2017b. UnceRtainty Analysis In CFD Verification and Validation, Methodology and Procedures. Technical Report, International Towing-Tank Conference (ITTC), URL: https://www.ittc.info/media/8153/75-03-01-01.pdf.

Armstrong, N., 2000. On the viscous resistance and form factor of high-speed Catamaran-ferry hull forms (Ph.D. thesis). University of New South Wales, URL: https://doi.org/10.26190/unsworks/4425.

Bailey, D., 1976. The NPL High Speed Round Bilge Displacement Hull Series: Resistance, Propulsion, Manoeuvring and Seakeeping Data. techreport 4, The Royal Institution of Naval Architects, URL: https://edisciplinas.usp.br/pluginfile.php/5797551/mod_resource/content/1/NPL.pdf.

Barber, C.B., Dobkin, D.P., Huhdanpaa, H.T., 1996. The quickhull algorithm for convex hulls. ACM Trans. Math. Software 22 (4), 469–483.

Blendermann, W., 1996. Wind Loading of Ships: Collected Data from Wind Tunnel Tests in Uniform Flow. techreport 574, Institut für Schiffbau der Universität Hamburg, Institut für Schiffbau, der Universität Hamburg, Lämmersieth 90, D-22305 Hamburg.

Brødrene, A., 2022a. Deliveries. URL: https://www.braa.no/fast-ferries.

Brødrene, A., 2022b. MS tyrhaug, vessel data. URL: https://www.braa.no/fast-ferries/ms-tyrhaug.

Carter, D.J.T., 1982. Prediction of wave height and period for a constant wind velocity using the JONSWAP results. Ocean Eng. 9 (1), 17–33. http://dx.doi.org/10.1016/0029-8018(82)90042-7, URL: https://www.sciencedirect.com/science/article/pii/0029801882900427.

Couser, P., 1996. An Investigation into the Performance of High-Speed Catamarans in Calm Water and Waves (Ph.D. thesis). University of Southampton, Department of Ship Science, URL: https://eprints.soton.ac.uk/459597/.

Couser, P.R., Molland, A.F., Armstrong, N.A., Utama, I.K.A.P., 1997. Calm water powering predictions for high-speed Catamarans. In: Proceedings of the Fourth International Conference on Fast Sea Transportation. In: FAST '97, URL: https://repository.tudelft.nl/islandora/object/uuid:d3fae17b-f723-4821-b29d-358970242c2b.

Couser, P.R., Wellicome, J.F., Molland, A.F., 1998a. Experimental measurement of sideforce and induced drag on Catamaran demihulls. Int. Shipbuild. Prog. ISP 45 (443), 225–235, URL: https://repository.tudelft.nl/islandora/object/uuid:9de6c067-32c7-4dc3-a22d-abb4d35836ea.

Couser, P.R., Wellicome, J.F., Molland, A.F., 1998b. An improved method for the theoretical prediction of the wave resistance of transom-stern hulls using a slender body approach. Int. Shipbuild. Progr. ISP 45, 331–350, URL: https://www.researchgate.net/publication/242218273_An_improved_method_for_the_theoretical_prediction_of_the_wave_resistance_of_transom-stern_hulls_using_a_slender_body_approach.

Cyberiad, 2015. Michlet 9.33 User's Manual. techreport, Cyberiad, URL: http://www.oscae.org/content/courses/shipdesign/michman_933.pdf.

Day, A.H., Doctors, L.J., 1997. Resistance optimization of displacement vessels on the basis of principal parameters. J. Ship Res. 41 (4), 249–259, URL: https://onepetro.org/JSR/article/41/04/249/174898/Resistance-Optimization-of-Displacement-Vessels-on.

Doctors, L.J., 2015. Hydrodynamics of High-Performance Marine Vessels. CreateSpace Independent Publishing Platform.

Doctors, L.J., Day, A.H., 1997. Resistance prediction for transom-stern vessels. In: Proceedings of the 4th International Conference on Fast Sea Transportation, FAST'97. pp. 743–750.

Doğrul, A., Kahramanoğlu, E., Çakıcı, F., 2021. Numerical prediction of interference factor in motions and added resistance for delft Catamaran 372. Ocean Eng. 223, 108687. http://dx.doi.org/10.1016/j.oceaneng.2021.108687, URL: https://www.sciencedirect.com/science/article/pii/S0029801821001220.

Eça, L., Hoekstra, M., 2008. The numerical friction line. J. Mar. Sci. Technol. 13, 328–345, URL: https://link.springer.com/article/10.1007/s00773-008-0018-1.

Faltinsen, O.M., 1990. Sea Loads on Ships and Offshore Structures, Vol. 1. Cambridge University Press.

Faltinsen, O.M., 2005. Hydrodynamics of High-SPeed Marine Vehicles. Cambridge University Press.

Faltinsen, O.M., Helmers, J.B., Minsaas, K.J., Zhao, R., 1991. Speed loss and operability of Catamarans and SES in a seaway. In: 1st International Conference on Fast Sea Transportation. In: FAST'91, Trondheim, pp. 709–726.

Faltinsen, O.M., Minsaas, K.J., Liapis, N., Skjørdal, S.O., 1980. Prediction of resistance and propulsion of a ship in a seaway. In: Proceedings of the 13th Symposium on Naval Hydrodynamics. Tokyo, pp. 505–529.

Førrisdal, E.W., 2018. Empirical Preidction of Residuary Resistance of Fast Catamarans. Norwegian University of Science and Technology, Department of Marine Technology, URL: https://ntnuopen.ntnu.no/ntnu-xmlui/bitstream/handle/11250/2564471/19424_FULLTEXT.pdf?sequence=1.

Friendship Systems, 2023. CAESES. URL: https://www.caeses.com/products/caeses/.

Godø, J.M., Steen, S., 2023. FASTSHIPS. URL: https://www.ntnu.edu/imt/software/fastships.

Grigson, C.W., 1999. A planar friction algorithm and its use in analysing hull resistance. Trans RINA 76–115.

Hoerner, S.F., 1965. Fluid-DYnamic Drag. Published by the Author.

Holling, H.D., Hubble, E.N., 1974. Model resistance data of series 65 hull forms applicable to hydrofoils and planing craft. resreport 4121, Naval Ship Research and Development Center.

Insel, M., 1990. An Investigation into the Resistance Components of High Speed Displacement Catamarans (Ph.D. thesis). University of Southampton, Factulty of Engineering and Applied Science, Department of Ship Science, URL: https://eprints.soton.ac.uk/462776/.

Isherwood, R.M., 1972. Wind resistance of merchant ships. Trans RINA 115, 327–338.

Jamaluddin, A., Utama, I.K.A.P., Widodo, B., Molland, A.F., 2013. Experimental and numerical study of the resistance component interactions of Catamarans. Proc. Instit. Mech. Eng. Part M: J. Eng. Maritime Environ. 227 (1), 51–60, URL: https://journals.sagepub.com/doi/full/10.1177/1475090212451694.

Jorde, J.H., 1991. The development of a 50 knot 40 m foilcat. In: Proceedings of the 1st International Conference on Fast Sea Transportation. In: FAST'91, vol.2, Trondheim, pp. 1093–1112.

Kanellopoulou, A., Zaraphonitis, G., Xing-Kaeding, Y., Papanikolaou, A., 2019. Parametric design and optimization of a battery-driven Catamaran in CAESES. In: CAESES User's Meeting 2019. Berlin, URL: https://www.friendship-systems.com/wp-content/uploads/2019/10/Kanellopoulou_Zaraphonitis_NTUA_Xing-Kaeding_Papanikolaou_Mittendorf_HSVA_parametric-design-and-optimization-of-a-battery-driven-{C}atamaran.pdf.

Katsui, T., 2005. The proposal of a new friction line. In: Fifth Osaka Colloquium on Advanced CFD Applications to Ship Flow and Hull Form Design. Osaka, Japan.

Lugni, C., Colagrossi, A., Colicchio, G., Faltinsen, O.M., 2004a. Numerical and Experimental Investigations on Semi-displacement Mono- and Multi-hulls. resreport, INSEAN, The Italian Ship Model Basin, URL: https://repository.tudelft.nl/islandora/object/uuid:5f58353c-6dcd-44dd-b997-12912842fa57.

Lugni, C., Colagrossi, A., Landrini, M., Faltinsen, O.M., 2004b. Experimental and numerical study of semi-displacement mono-hull and Catamaran in calm water and incident waves. In: Proceedings of the 25th Symposium on Naval Hydrodynamics. St. John's, Canada.

Maki, K.J., Doctors, L.J., Beck, R.F., 2007. On the profile of the flow behind a transom stern. In: 9th International Conference on Numerical Ship Hydrodynamics. Ann Arbor, Michigan, URL: https://www.researchgate.net/profile/Lawrence-Doctors/publication/292839897_On_the_profile_of_the_flow_behind_a_transom_stern/links/60a619da45851505a0e4b8b8/On-the-profile-of-the-flow-behind-a-transom-stern.pdf.

Maki, K.J., Troesch, A.W., Beck, R.F., 2008. Experiments of two-dimensional transom stern flow. J. Ship Res. 52 (04), 291–300. http://dx.doi.org/10.5957/jsr.2008.52.4.291, URL: https://onepetro.org/JSR/article/52/04/291/175082/Experiments-of-Two-Dimensional-Transom-Stern-Flow.

Marwood, W.J., Bailey, D., 1969. Design data for high-speed displacement hulls of round-bilge form. resreport 99, National Physical Laboratory, Ship Division.

Michell, J.H., 1898. The wave-resistance of a ship. Lond. Edinburgh Dublin Philos. Mag. J. Sci. 45 (272), 106–123. http://dx.doi.org/10.1080/14786449808621111.

Miljodirektoratet, 2019. Utviklingskontrakt for hurtigbåt. URL: https://www.miljodirektoratet.no/ansvarsomrader/klima/for-myndigheter/kutte-utslipp-av-klimagasser/klimasats/2017/utviklingskontrakt-for-hurtigbat/#.

Minsaas, K.J., 1993. Design and development of hydrofoil Catamarans in Norway. In: Proceedings of the 2nd International Conference of Fast Sea Transportation. In: FAST'93, Yokohama, Japan, pp. 83–100.

Mittendorf, M., Papanikolaou, A.D., 2021. Hydrodynamic hull form optimization of fast Catamarans using surrogate models. Ship Technol. Res. 68 (1), 14–26, URL: https://www.tandfonline.com/doi/full/10.1080/09377255.2020.1802165.

Molland, A.F., Barbeau, T.-E., 2003. An investigation into the aerodynamic drag on the superstructure of fast Catamarans. Trans. R. Instit. Naval Archit. Part A: Int. J. Marit. Eng. 145, 29–39, URL: https://eprints.soton.ac.uk/22232/.

Molland, A.F., Lee, A.R., 1995. Resistance Experiments on a Series of High Speed Displacement Catamaran Forms: Variation of Prismatic Coefficient, Ship Science Report. resreport 86, University of Southampton, URL: https://eprints.soton.ac.uk/46460/1/086.pdf.

Molland, A.F., Lee, A.R., 1997. An investigation into the effect of prismatic coefficient on Catamaran resistance. Trans RINA 139, 157–165.

Molland, A.F., Wellicome, J.F., Couser, P.R., 1994a. Resistance Experiments on a Systematic Series of High Speed Displacement Catamaran Forms: Variation of Length-Displacement Ratio and Breadth-Draught Ratio, Ship Science Report. resreport 71, University of Southampton, Department of Ship Science, URL: https://eprints.soton.ac.uk/46442/1/071.pdf.

Molland, A.F., Wellicome, J.F., Couser, P.R., 1994b. Theoretical Prediction of the Wave Resistance of Slender Hull Forms in Catamaran Configurations, Ship Science Report. resreport 72, University of Southampton, Department of Ship Science, URL: https://eprints.soton.ac.uk/46441/1/072.pdf.

Müller-Graf, B., 1993. SUS a - the scope of the VWS hard chine Catamaran hull series '89. In: Proceedings of the 2nd International Conference on Fast Sea Transportation. In: FAST'93, vol.1, Yokohama, Japan, pp. 223–238.

Müller-Graf, B., 1994. General resistance aspects of advanced fast marine vehicles. In: Short Course on Design of Advanced Fast Marine Vehicles, Versuchsanstalt für Wasserbau und Schiffbau. Hamburg, Germany.

Müller-Graf, B., Radojčić, D., Simić, A., 2002. Resistance and propulsion characteristics of the VWS hard Chine Catamaran Hull series '89. Trans. - Soc. Naval Archit. Mar. Eng. 110, 1–27.

NORDFORSK, 1987. Assessment of Ship Performance in a Seaway. results of a Nordic Co-Operative Project on Seakeeping Performance of Ships. resreport 1, SSPA, MARINTEK, SL, VTT, Sortedam Dossering 19, DK-2200 Copenhagen N.

Nordström, H.F., 1951. Some Tests with Models of Small Vessels. resreport 19, SSPA, Göteborg.

Oura, T., Ikeda, Y., 2008. Maneuverability of a wavepiercing high-speed Catamaran at low speed in strong wind. In: Proceedings of the International Conference on Marine Research and Transportation. pp. 83–88. http://dx.doi.org/10.14856/conf.4.0_17, URL: http://www.icmrt07.unina.it/Proceedings/Papers/A/35.pdf.

Papanikolaou, A., Xing-Kaeding, Y., Strobel, J., Kanellopoulou, A., Zaraphonitis, G., Tolo, E., 2020. Numerical and experimental optimization study on a fast, zero emission Catamaran. J. Mar. Sci. Eng. 8 (9), 657–675. http://dx.doi.org/10.3390/jmse8090657, URL: https://www.mdpi.com/2077-1312/8/9/657.

Rambech, H.J., 1998. Empirisk Motstandsberegning for Hurtiggående Katamaraner. (Project Thesis). Norwegian University of Science and Technology.

Sahoo, P.K., Browne, N.A., Salas, M., 2004. Experimental and CFD study of wave resistance of high-speed round bilge Catamaran hull forms. In: Bertram, V. (Ed.), Proceedings of the 4th International Conference on High Performance Marine Vehicles. HIPER, Rome, Italy, pp. 509–516, URL: https://www.researchgate.net/profile/Prasanta-Sahoo-2/publication/266181362_Experimental_and_CFD_Study_of_Wave_Resistance_of_High-Speed_Round_Bilge_Catamaran_Hull_Forms/links/561ea4fb08ae50795aff288d/Experimental-and-CFD-Study-of-Wave-Resistance-of-High-Speed-Round-Bilge-Catamaran-Hull-Forms.pdf.

Sahoo, P.K., Salas, M., Schwetz, A., 2007. Practical evaluation of resistance of high-speed Catamaran hull forms - part I. Ships Offsh. Struct. 2 (4), 307–324, URL: https://www.tandfonline.com/doi/full/10.1080/17445300701594237.

Savitsky, D., 1988. Wake shapes behind planing hull forms. In: Proceedings of the International High Performance Vehicle Conference, VII. Shanghai, China, pp. 1–15.

Shi, G., Priftis, A., Xing-Kaeding, Y., Boulougouris, E., Papanikolaou, A.D., Wang, H., Symonds, G., 2021. Numerical investigation of the resistance of a zero-emission full-scale fast Catamaran in shallow water. J. Mar. Sci. Eng. 9 (6), http://dx.doi.org/10.3390/jmse9060563, URL: https://www.mdpi.com/2077-1312/9/6/563.

Shippax, 2021. In: Holthof, P. (Ed.), Shippax Market 21, the 2020 Ferry, Cruise, Ro-RO and High-SPeed Year in Review with Analyses and Statistics. Shippax, Halmstad, Sweden.

Steen, S., Minsaas, K., 2014. Motstand og propulsjon, propell- og foilteori. Lecture notes in TMR4247 marine technology 3 - hydrodynamics, NTNU. Otto Nielsens Veg 10, 7052 Trondheim.

Subramanian, V.A., Joy, P., 2004. A method for rapid hull form development and resistance estimation of Catamarans. Mar. Technol. Soc. J. 38 (1), 5–11, URL: https://www.ingentaconnect.com/content/mts/mtsj/2004/00000038/00000001/art00002.

Sundvor, I., Thorne, R.J., Danebergs, J., Aarskog, F., Weber, C., 2021. Estimating the replacement potential of norwegian high-speed passenger vessels with zero-emission solutions. Transp. Res. Part D: Trans. Environ. 99, http://dx.doi.org/10.1016/j.trd.2021.103019, URL: https://www.sciencedirect.com/science/article/pii/S1361920921003175.

Svenneby, E.J., Minsaas, K.J., 1992. Foilcat 2900, design and performance. In: Proceedings of the Third Conference on High-SPeed Marine Craft, no. 6. Norwegian Society of Chartered Engineers, Oslo.

Taravella, B.M., McKesson, C.B., Vorus, W.S., 2012. A very simple model for the wake hollow behind a high-speed displacement hull. Naval Eng. J. 124 (3), 85–91, URL: https://www.ingentaconnect.com/content/asne/nej/2012/00000124/00000003/art00016.

The SciPy Project, 2023. Scipy documentation. URL: https://docs.scipy.org/doc/scipy/index.html.

TrAM, 2022. World's first zero emission fast ferry has been named. URL: https://tramproject.eu/2021/02/16/worlds-first-zero-emission-fast-ferry-has-been-named/.

Tuck, E.O., 1987. Wave Resistance of Thin Ships and Catamarans, Report T8701. resreport, University of Adelaide, Applied Mathematics Department, URL: http://www.maths.adelaide.edu.au/yvonne.stokes/Tuck/pdfiles/t8701.pdf.

Utama, I.K.A.P., Molland, A.F., 2001. Experimental and numerical investigations into Catamaran viscous resistance. In: Proceedings of the Sixth International Conference on Fast Sea Transportation. In: FAST 2001, Southampton, UK, pp. 295–306, URL: http://eprints.soton.ac.uk/id/eprint/22216.

van't Veer, I.R., 1998a. Experimental Results of Motions and Structural Loads on the 372 Catamaran Model in Head and Oblique Waves, Report 1130. resreport, Delft University of Technology, Faculty of Mechanical Engineering and Marine Technology, Ship Hydromechanics Laboratory, 2600 AA Delft, The Netherlands, URL: https://research.tudelft.nl/en/publications/experimental-results-of-motions-and-structural-loads-on-the-372-c.

van't Veer, I.R., 1998b. Experimental Results of Motions, Hydrodynamic Coefficients and Wave Loads on the 372 Catamaran Model, Report 1129. resreport, Delft University of Technology, Faculty of Mechanical Engineering and Marine Technology, Ship Hydromechanics Laboratory, 2600 AA Delft, The Netherlands, URL: https://research.tudelft.nl/en/publications/experimental-results-of-motions-hydrodynamic-coefficients-and-wav.

Vernengo, G., Brizzolara, S., 2015. Resistance and seakeeping optimization of a fast multihull passenger ferry. Int. J. Offs. Polar Eng. 25 (01), 26–34, URL: https://onepetro.org/IJOPE/article/25/01/26/26446/Resistance-and-Seakeeping-Optimization-of-a-Fast.

Vernengo, G., Villa, D., Bruzzone, D., Bonfiglio, L., 2021. A study on the added resistance of a catamaran advancing in waves considering variations of both operating and geometric parameters. Ships Offshore Struct. 16 (4), 334–352. http://dx.doi.org/10.1080/17445302.2020.1727180.

Wang, H., Zhu, R., L., Z., M., G., 2022. Experimental and numerical investigation on the resistance characteristics of a high-speed planing Catamaran in calm water. Ocean Eng. 258, 111837. http://dx.doi.org/10.1016/j.oceaneng.2022.111837, URL: https://www.sciencedirect.com/science/article/pii/S0029801822011805.

Werenskiold, P., 1990. Design tool for high speed slender Catamarans. In: High Speed Marine Craft, no. 2447. MARINTEK A/S OCEAN LABORATORIES, Trondheim Norway, Kristiansand, Norway, URL: https://repository.tudelft.nl/islandora/object/uuid:94dea358-8030-4d6b-a85e-cfa2204f1208.

Wigley, W.G.S., 1942. Calculated and measured wave resistance on a series of forms defined algebraically, the prismatic coefficient and angle of entrance being varied independently. Trans RINA 84, 52–74.

Yeh, H.Y.H., 1965. Series 64 resistance experiments on high-speed displacement forms. Mar. Technol. SNAME News 2 (03), 248–272. http://dx.doi.org/10.5957/mt1.1965.2.3.248, URL: https://onepetro.org/MTSN/article/2/03/248/169061/Series-64-Resistance-Experiments-on-High-Speed.

Zhang, C., He, J., Ma, C., Francis, N., Wan, D., Huang, F., Yang, C., 2015. Validation of the Neumann-Michell theory for two catamarans. In: Proceedings of the Twenty-Fifth International Ocean and Polar Engineering Conference, ISOPE, no. ISOPE-I-15-022. Kona, Hawaii, USA, pp. 1018–1024, URL: https://onepetro.org/ISOPEIOPEC/proceedings/ISOPE15/All-ISOPE15/ISOPE-I-15-022/14410.